# DEVELOPMENT, CALIBRATION AND EVALUATION OF A TELEMETRIC TRANSDUCER FOR PATELLOFEMORAL FORCE MEASUREMENT IN A HUMAN KNEE

by

Eric T. Hansen

A thesis submitted to the Faculty and Board of Trustees of the Colorado School of Mines in partial fulfillment of the requirements for the degree Master of Science in Engineering Systems.

Golden, Colorado

Date_____

Signed: _____
Eric T. Hansen

Approved: _____
Dr. Joel Bach
Thesis Advisor

Approved: _____
Dr. Rahmat Shoureshi
Thesis Advisor

Golden, Colorado

Date_____

_____
Dr. David Munoz
Acting Director
Engineering Division

## ABSTRACT

A telemetric knee is being developed with the intent of measuring and predicting patellofemoral and tibiofemoral forces in the knee joint following total knee arthroplasty (TKA). A patellar transducer has been developed that is implanted during a TKA in place of the posterior half of the patella, and measures the magnitude and location of the patellofemoral force. With appropriate kinematic modeling, tibiofemoral forces can be resolved from this data as well. The transducer was designed using Finite Element Analysis (FEA) to optimize the thickness and geometry of the transducer to maximize sensitivity yet still provide appropriate structural integrity.

Calibration of the transducer is accomplished by rotating the orthogonal coordinate system off-axis from the normal load such that calibration loading vectors are all at equal angles from the transducer plane. This alleviates stress-concentration artifacts that may be present when loading the transducer along its plane. The transducer is cyclically loaded with a known magnitude along all three axes. This data is then used to derive a calibration matrix that can be applied to any force vector. A wireless data transfer system is used in the current prototype, and an embedded wireless system is proposed. *In situ* testing in a cadaver leg segment illustrates the ability of the transducer to measure relative load, but brings to light concerns regarding repeatability and temperature sensitivity. Further *in vitro* testing evaluates probable causes of these problems and ways to address them. Design modifications based on the experimental analysis of this research have been recommended. These modifications should improve robustness, repeatability and sensitivity to such variables as temperature.

## TABLE OF CONTENTS

## LIST OF FIGURES

## LIST OF TABLES

## ACKNOWLEDGEMENT

I would like to thank NAVIGANT BIOTECHNOLOGIES and its employees for their support of my degree pursuits, of which this project is a large part. In addition, I wish to extend my sincere thanks to my advisors Dr. Joel Bach and Dr. Rahmat Shoureshi for their support and incite in making this project a success, and Todd Baldini and Dr. Donald Eckhoff of the University of Colorado Health Sciences Center Opthopaedic Biomechanics Laboratory for their help in performing testing associated with this project.

Most importantly, I'd like to thank my wife Stephanie for her endless support and encouragement, and my two girls Caitlynn and Meghan for allowing my absence all of those late nights and weekends.

# Chapter 1

## INTRODUCTION

Total knee replacement (also known as total knee arthroplasty, or TKA) surgery represents more than 300,000 orthopedic surgeries a year in the U.S. alone, accounting for over $2 billion in medical expenses [1, 2]. Knee degeneration can be caused by many forms of arthritis—both genetic and environmental in nature. The most common causative disease of joint destruction is osteoarthritis, which causes the degeneration of articular cartilage in joints. While there is genetic predisposition to this disease, it is exacerbated by high impact use, such as running, skiing, and even obesity [3]—things that are not necessarily related to genetics. Common symptoms of joint degeneration include severe pain, inflammation, and joint instability and locking. Eventually this condition leads to reconstructive surgery of the knee joint using artificial implants. Knee reconstruction involves removal of the diseased articular surfaces of the tibia, femur and patella, followed by replacement with metal and plastic components. Many knee reconstructions are partial, in which only one or two of the articular surfaces are replaced, although total reconstruction remains the preferred course of treatment. The anatomy of a normal knee and a reconstructed knee are illustrated in Figure 1.1.

Today, knee reconstruction is a highly advanced procedure, and the materials and geometries used are truly state of the art. Although implant manufacturers claim a life expectancy of upwards of 15 years, nearly 15 percent of today's implants fail in the first 10 years [4]. Failures are due to a number of causes including bone-metal separation, articulating surface wear, and poor knee geometry/function replication. All three failure modes are related to the internal knee contact forces and the loading characteristics of the artificial components [5]. The ability to monitor the internal contact forces *in vivo* following a TKA procedure could help diagnose aberrant loading conditions earlier, thus

potentially eliminating many implant failures. Additionally, this joint-loading data may be useful for modeling future implant designs, leading to artificial components that replicate normal knee function more closely.

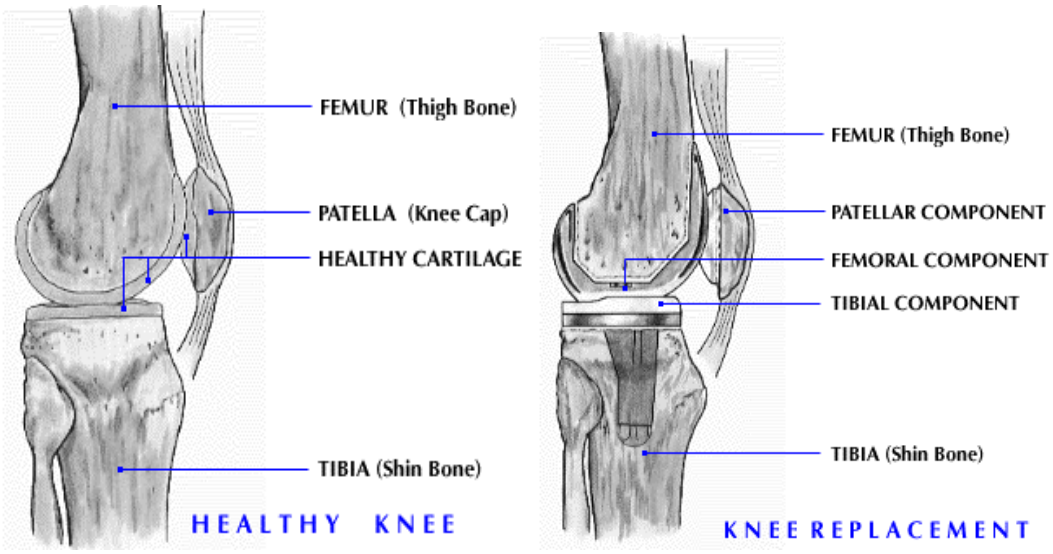


Figure 1.1: Healthy and reconstructed knee joints.

The geometry of the knee dictates certain feasible locations for an implanted force transducer. The two joint forces of interest are between the tibia and femur (tibiofemoral) and between the patella and femur (patellofemoral). Instrumentation of the femur would require either functional isolation of the two contact regions or settling for a combined force output. The former would be extremely difficult and would likely be mechanically unstable from a joint function perspective. The latter would provide less useful information as a diagnostic and design tool. Alternatively, either the tibia or the patella can be instrumented with the concession that only one of the contact forces can be

directly measured. The second force can then be estimated using kinematic knee models (either existing or to-be-developed). Alternatively, both structures could be instrumented if so desired. Instrumentation of the patella, and thus measurement of patellofemoral forces, was chosen as the system for this project, as it is a novel approach to the problem.

The original intended application of this project was to use the data generated from the patellar transducer to calculate the tibiofemoral contact force using 2-dimensional or 3-dimensional knee models. While this may be a plausible application, the general consensus in the field [6] is that mathematical models of the knee provide rough estimations only, and are not considered precise enough to accurately calculate a tibiofemoral force given the patellofemoral force. This is further complicated by the knowledge that every individual's knee geometry is slightly different, every TKA implant design is geometrically different, and degradation of the joint over time (precisely what we are attempting to measure) will further change the joint geometry and invalidate the mathematical model. Current research by D'Lima et al [7, 8] on an instrumented tibial implant directly measure the tibiofemoral force, giving an accurate depiction of the joint dynamics between those two components, therefore rendering the instrumented patella obsolete for this originally intended use.

However, it is of the opinion of this researcher that the diagnostic usefulness of the patellofemoral contact force is significantly high to support continued development of this project [9, 10]. Among the complications of TKA that are currently reported, 30% [11] are directly related to the patellofemoral joint. These include anterior knee pain, patellar subluxation and dislocation as well as abnormal polyethylene wear and damage of the patellar component. Even if advancements in knee modeling never make it possible to accurately calculate the tibiofemoral force, the advancements that can be made in TKA diagnosis and design just from the patellofemoral component are significant enough for this project to be considered valuable.

The intent of this project is to design an implant that can be used in conjunction with a full knee reconstruction, and is able to measure the patellofemoral forces occurring within the reconstructed knee. The final device should be able to resolve three-dimensional patellofemoral contact force, be capable of transmitting this loading data at least ten feet, and be either self-powered or have an extra-corporeal power source. In addition, the device and all associated electronics should be fully contained in the patellar implant portion of the artificial joint. Previous work associated with this project investigated the feasibility of a kinematic model of the knee relating the patellofemoral force to the tibiofemoral force in two dimensions. The device will allow the study of knee joint kinematics and dynamics *in vivo* under weight-bearing conditions, an approach that differs from previous *ex vivo* implant-modeling methods. This data will allow the treating physician to monitor the welfare of the artificial joint, and can aid researchers in improving the geometry and/or materials of knee implants to best suit the observed articular contact forces.

This thesis represents work performed in the second phase of a multi-phase project, and describes the development of a prototype patellar transducer and the calibration and testing procedures associated with reducing the design to practice. Telemetry and power systems for the patellar device have been explored extensively—both experimentally and through literature research—the results of which are described herein. The configuration of the current functional prototype is discussed, along with the design modifications that are necessary for the next generation device.

# Chapter 2

# BACKGROUND

The concept of a telemetric knee was first proposed by Dr. Rahmat Shoureshi, PhD, Professor of Engineering at Colorado School of Mines. The first phase of the project, as supervised by Dr. Shoureshi, included transducer design, exploratory work with telemetry and power systems, and development of a two-dimensional mathematical model of the knee [12]. This chapter represents the work that was performed in the first phase of this project, as well as literature review that was conducted as part of this (the second) phase. Additional research and evaluation has been conducted for each of these systems, and is detailed in Chapter 3.

## 2.1 Telemetered Knee Review

Measurement of both the patellofemoral and tibiofemoral joint reaction forces have been performed in vitro on human cadaver knee specimens for over twenty years, and more recently, temporary force and pressure measurement systems have been used during operation to gage joint performance [12]. In 1996, an initial publication was released by Kaufman et al [7] describing the development and testing of a strain-based device to measure tibiofemoral forces. The device utilized 32 strain gages to measure the magnitude and location of the tibiofemoral force. The extensive electronics required the entire volume of the artificial tibial component, making the envisioned telemetry system seemingly impossible. Later publications and presentations [6, 8, 13] describe further development of the device and conversion to a telemetric data transfer system. By redesigning the architecture of the tibial component and extensive use of finite element analysis techniques, the instrumentation was reduced to four strain gages mounted in a rosette on the tibial platform, and a custom telemetry system (MicroStrain Industries,

Williston, VT) enclosed in the stem. Reported accuracy of the latest tibial tray transducer is ±1.2% for force magnitude, and ±1 mm for location [8].

A similar instrumented tibia implant is being developed at the Free University of Berlin [14] using the same principles of force transduction and telemetry pioneered by Bergman et al in the 1990's for an instrumented hip implant [15, 16, 17]. This program was initiated in 2003 and is still in its infancy. There are currently no visible research efforts focusing on a telemetric patella outside of this one.

### 2.2 Patellar Transducer Design

The patellar implant utilized in this project consists of two parts, a metal transducer that attaches to the bone, and an Ultra-High Molecular Weight Polyethylene (UHMWPE) cap that articulates with the femoral component of the TKA. Initial transducer prototypes consisted of a central post affixed to a circular plate. Normal forces were captured using strain gages mounted to the undersurface of the plate, while side forces were measured using bending-beam effects in the post. The post was threaded for attachment of the polyethylene cap. Three different instrumentation configurations of the post-style transducer were built and tested, the third of which was instrumented with just three gages on the underside of the base [15]. Load testing was performed using free weights suspended only by the transducer—this was done for both normal and side-loading conditions. These tests indicated that the post design was adequate for measuring both normal and side forces, and that the three-gage rosette was a valid method of minimizing the instrumentation. During the side-loading testing, it became obvious that the threaded post style transducer would not be adequate, as the threaded interface between the polyethylene dome cap and the transducer was much too fragile. After careful consideration of the articulation between the two materials, it was decided that the contact area between the transducer and the cap must be maximized, which would not be possible using a post-style transducer.

Several plate-style transducers were designed (Solid Edge, UGS, Cypress CA) with the purpose of maximizing the contact area between the transducer and the polyethylene cap. The geometry of these plate-style transducers is more complex than the original post-style, rendering previous mathematical models invalid and requiring higher level analysis. To assist in analysis of stress-strain profiles of the transducer models, a finite element analysis tool was employed (Visual Nastran, MSC Software, San Mateo CA). Twenty-three designs were modeled—variations included: differences in plate thickness, variations in the height of the metal-polyethylene articular cylinder, the geometry of the model's undersurface, and the depth of the center cutout. Common design factors included maximum polyethylene volume, maximum polyethylene-metal contact area, minimal von Mises stress, and maximum strain gage sensitivity. The objective of these studies was to determine which design created sufficient strain to be useful as a sensor, as well as to keep the stress low enough to withstand high-magnitude repetitive loading. Figure 2.1 shows the final design in 3D mesh form. This configuration was evaluated for stress and strain profile at 1x, 2x, 4x and 6x body weight, where body weight was taken to be 180 lbs (800 N). The strain and stress profiles for the device at 4x body weight are illustrated in Figures 2.2 and 2.3. Additional virtual loading studies were performed to compare ASTM F799 Cobalt-Chromium, the anticipated final design material, and 316L Stainless, the intended prototype material. For conditions expected during calibration and feasibility studies (2x body weight, maximum), 316L appeared to be acceptable, and four prototypes were built.

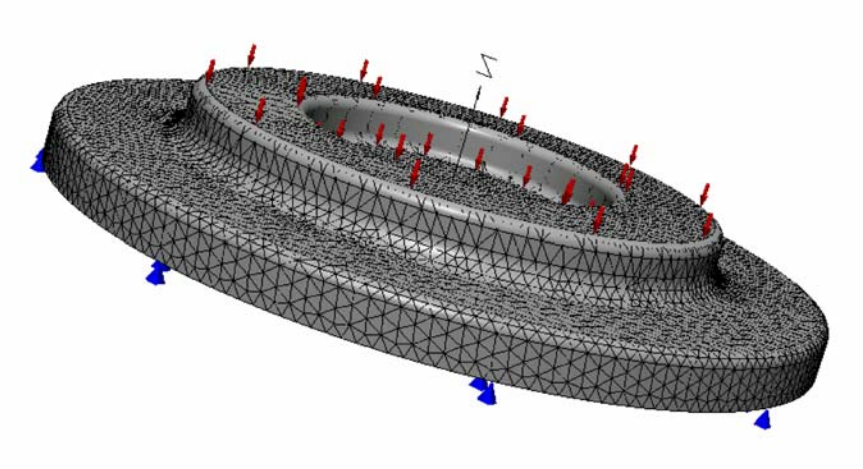

Figure 2.1: Final transducer design, FEA mesh representation.

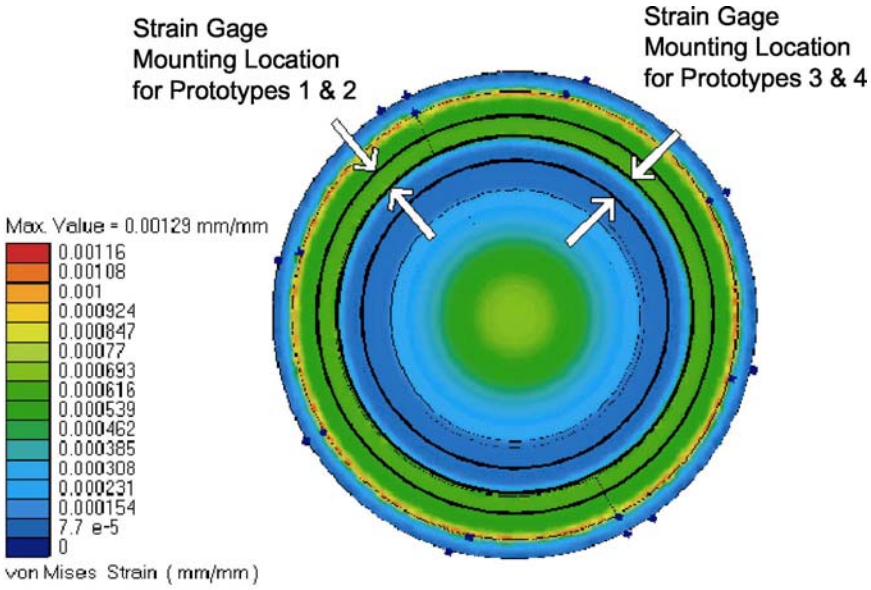


Figure 2.2: Strain profile of the final design, with gage placement.

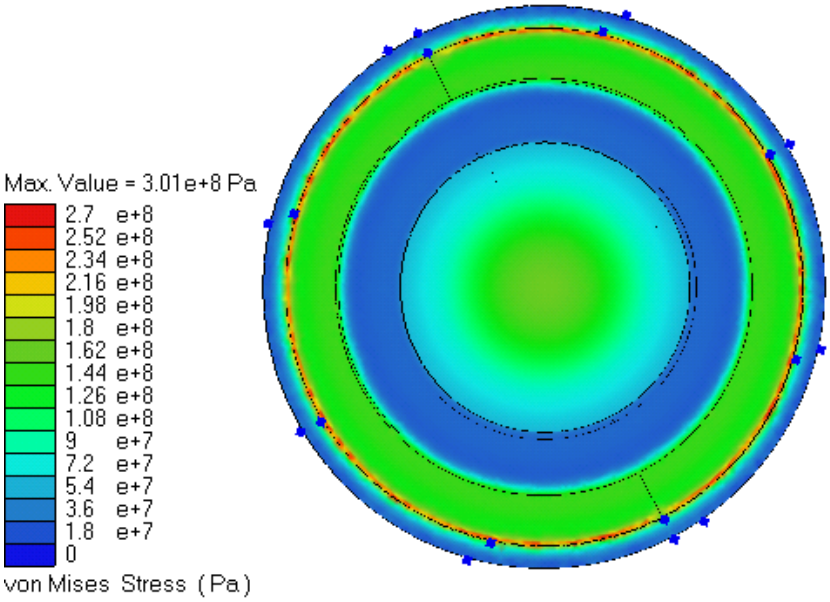


Figure 2.3: Stress profile of the final design.

As illustrated in Figure 2.2, there were two strain gage mount locations used in prototype construction. The mount location in prototypes 1 and 2 had higher sensitivity to loading, but with higher error, while the mount location for prototypes 3 and 4 had reduced error, but also reduced sensitivity. It was not obvious from the FEA work which mounting location would be preferred in the final design, so prototypes were constructed both ways. Each transducer was instrumented with three strain gages (350 Ω, 150 gf semiconductor gages, Entran Sensors, Fairfeld NJ) in a floret at 120$^{o}$ angular separation. This gage placement is consistent with the pattern used in the final prototype post-style transducer, and is as described by Bergmann et al.

In addition to the transducer plate, a base plate was designed to protect the transducer from biological fluids and provide secure attachment to the bone. In the early prototypes, strain data will be transferred from the transducer via wire, so the base plate also must provide a hermetic seal around the wire exit. The bone articulation was designed to be similar to existing patellar implants with a cross-style protrusion that would eventually be coated to promote bone in-growth. The wire feed-through hole was hermetically sealed, and the two plates were laser welded together. Following assembly, the four prototype transducers were tested for their response to load, and an initial calibration was performed on each transducer.

## 2.3 Telemetry System Review

### 2.3.1 Previous Work

In the first phase of this project, a custom radio-frequency telemetry system was designed and built utilizing the Colpitz oscillator circuit [12, 15]. Strain gage signal resolution was accomplished using the current-difference principle instead of the traditional Wheatstone bridge method. This methodology provides for stable output current under varying voltage conditions and requires considerably less power [15]—both of which are important concerns for an implanted device where power may be widely variable. To control the amplitude modulation of the pulse train, a 555 timer was connected between the strain gage current sources and the oscillator circuit. This allowed for cycling between the three strain channels, as well as pulsed gage power consumption, keeping the overall power requirements at a minimum. The advantages of this homemade transmitter were that power requirements and transmission distance could be custom designed for this application. The disadvantage was the large amount of space that this circuitry would require, making it impossible to fit within the transducer shell.

### 2.3.2 Current Work

Several commercial technologies for wireless digital data transmission were investigated on the literature level for possible application in this program. The three most promising systems are BlueTooth Wireless (Bluetooth SIG, Overland Park, KS) [18, 19], CDMA ( Qualcomm Inc, San Diego, CA) [20], and SmartChips (IBM, Armonk, NY and Phillips Semiconductor, Cupertino, CA) [21]. All of these systems facilitate the transfer of large quantities of digital data over varying distances using a very small chip. The challenge of any of these technologies would be on-board A/D conversion of either the gage resistance or the voltage drop across a bridge, and the reduction of these technologies, designed for large sets of data, to use with a three-channel stream. While these technologies are powerful and can potentially meet the size and power requirements of this project, the development necessary to implement any of these technologies into this project is well beyond the scope of this thesis. Therefore it was decided to keep these technologies as potential options for future discussions, while proceeding with development and testing at this phase using conventional biotelemetry systems [8, 22].

MicroStrain Industries specializes in strain telemetry devices for orthopedic implantation, and has two off-the-shelf products that meet many of the needs of this project. The development-level device, StrainLink (Figure 3.4), is inexpensive, has three full differential channels, a 300Hz maximum sample rate, a 20 foot transmission distance, and is easily acquired into LabView. The customizable EmbedSense is designed for biomedical implantation and has similar performance specifications to the StrainLink platform. While the standard production design of EmbedSense (Figure 3.4) will not fit into the patellar transducer package, it can be simplified and miniaturized to roughly 0.75 in. diameter and 0.125 in. thickness, which could fit into the transducer housing with some redesign. The StrainLink system has been implemented into the testing and development of the current prototype transducers, with the intent to work in conjunction with MicroStrain to design the EmbedSense device into the next generation transducer.

Specific designs have not been considered during preliminary discussions with MicroStrain, pending financial commitment.

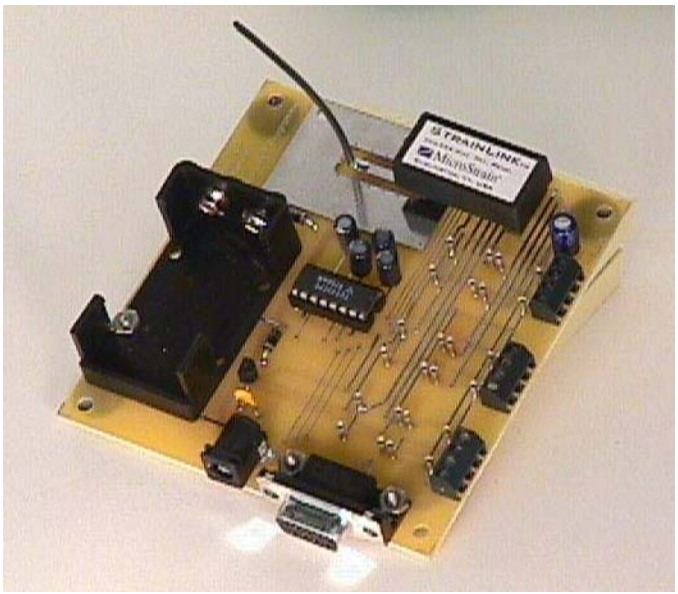


Figure 2.4: MicroStrain StrainLink transmitter and prototyping board.

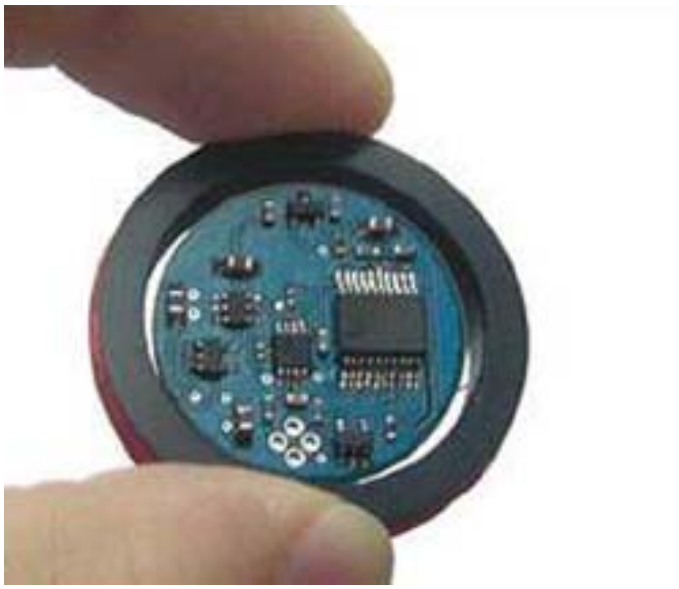

Figure 2.5: MicroStrain EmbedSense transceiver with induction coil.

**2.4 Power System Review**

Device power has been a formidable challenge in this project, as well as in other *in vivo* instrumentation devices. Battery power is not desirable due to the inevitable finite lifespan and the difficulties involved in mechanically loading a battery [23]. The typical power source for an implanted device is inductive power [24]. This utilizes magnetic coupling to transmit power transcutaneously—it is often used in association with an inductive telemetry system. Because this system has been investigated by other research teams with varying degrees of success, and due to unanswered concerns regarding the impact of electromagnetic fields on human tissues, the intent was to develop a novel system that would make the transducer truly self-powered. However, due to the complexities that remain with a power system, and the relative readiness of the rest of the device, the next generation transducer prototypes will likely incorporate an inductive power system, at least for interim use.

The long-term solutions to the power problem are a kinetic generator [12, 25, 26] or a chemical system [27, 28]. Any kinetic system would still require some type of battery or capacitive device to store power as it is generated, which still poses spatial and mechanical issues for this device. Furthermore, the plane of the transducer lies in a motion field that does not generate significant kinetic energy [12]. Kinetic devices function by swinging a weight across a coil, thus generating charge. Because the patellar transducer would be vertical during most normal activity, the plane of motion is far too small to generate much movement or energy. Future advances in kinetic power technology may eliminate these challenging issues. Chemical power conversion remains an interesting option, but the biochemistry behind this technology is still in its infancy and is probably several years out.

### 2.5 Two-Dimensional Knee Model

A two-dimensional mathematical model for relating the patellofemoral force and knee flexion angle to the tibiofemoral contact force was generated in the first phase of this project [12]. The model was constructed using literature references to force ratios within the normal knee joint [29, 30], and TKA kinematic data obtained from fluoroscopy images from five subjects. Figure 2.6 shows the model and relevant force vectors. The resulting model yielded theoretical tibiofemoral contact forces that were close in magnitude to published values—indicating that this method of resolving the tibiofemoral force may be a viable option given adequate knowledge of implant geometry and the ability to measure flexion angle. It may also be feasible to substitute the three-dimensional patellofemoral force for the two-dimensional force plus flexion angle to resolve the tibiofemoral contact force. Although the calculated contact force values agreed with published values, the use of force ratios from a normal knee is somewhat disconcerting, since one of the primary concerns of this project is the unknown nature of

force dynamics within a TKA. Assuming normal-knee kinematics may not lead to a device that addresses the original problem. Nonetheless, the working two-dimensional model is considered an acceptable start, subject to reevaluation pending the status of the transducer/telemetry unit.

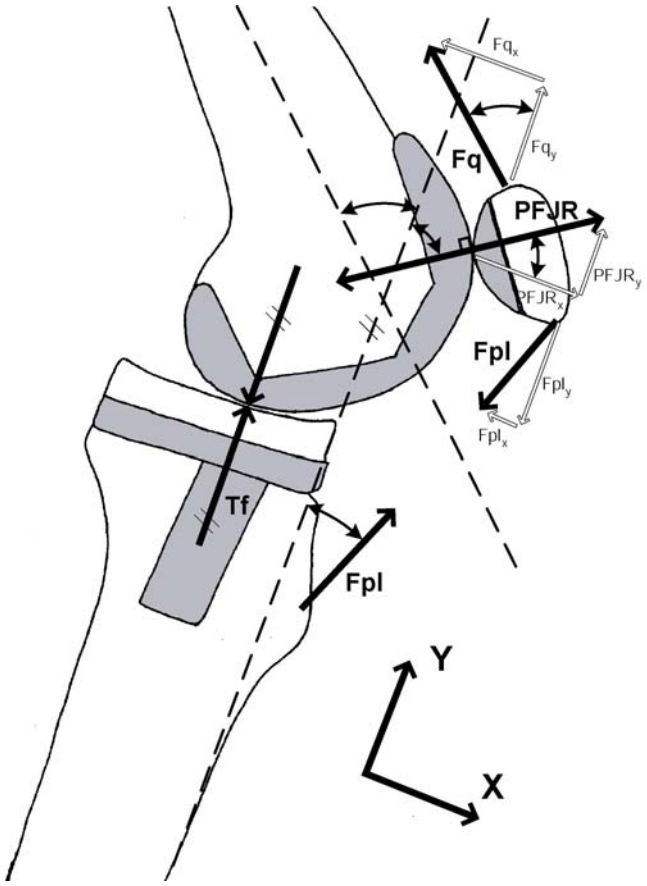


Figure 2.6: Two-dimensional knee model.

# Chapter 3

# SYSTEM DEVELOPMENT

The remainder of this thesis represents work performed in this, the second, phase of a multi-phase project. The goals of this phase included further reduction of the systems investigated previously to a working-practice design, development of a reproducible calibration procedure, and experimental investigation of the feasibility of the prototype system design. This chapter presents the research and experimentation performed that is relevant to the design and development of the Telemetric Knee System. The final configuration of the telemetric knee as used in calibration and feasibility testing is described in detail.

## 3.1 Transducer Signal Conditioning Design

The four prototype transducers designed and fabricated in the first phase of this project were completed just a few weeks prior to the completion of that phase. Consequently, minimal evaluation of the final prototype transducers was performed including normal loading studies using free weights, and calibration testing as described in section 4.2. The first experiments conducted during phase 2 of the project involved replication of those experiments to determine whether the results were repeatable. Immediate observations regarding transducer output drift and hysteresis, Wheatstone bridge instability, and inconsistent signal conditioning and data acquisition methods in the original testing, led to the following body of work.

The resistance change in each strain gage is transduced using a ¼ active arm Wheatstone bridge circuit. Initial stability testing and force response testing of the transducers yielded disappointing results. The drift in each channel was 8-12% in a temperature-stable environment, several of the channels showed significant hysteresis

when subjected to cycled loading, and some channels showed no response to loads up to 100N. Several iterations of the Wheatstone bridge circuit were tested in an effort to minimize the drift. The final configuration chosen is illustrated in Figure 3.1. The connection wire from the transducer to the transduction circuit was a three-wire design. This was done to reduce capacitance effects caused by the wire. The active arm of the bridge was constructed with 1% tolerance metal foil resistors, matched to the unloaded resistance of each gage of each transducer (280-340 ohm). The balance arm of the bridge was constructed with 3.00 kOhm 0.1% tolerance resistors. The higher resistance value was used to minimize current in the transducer, and thus minimize self-heating. The tighter tolerance was used to minimize fluctuation on the balance arm of the bridge. Implementation of these steps reduced the drift to less than 1% of initial gage output.

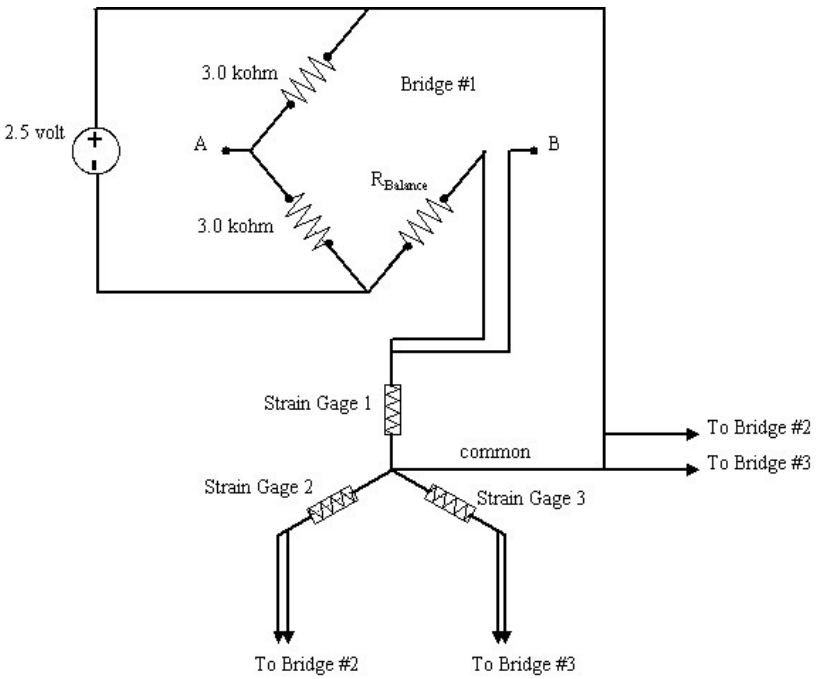


Figure 3.1: Three-wire bridge circuit design.

One of the most important variables for minimizing transducer drift was ambient temperature. Temperature compensation was not incorporated into the original implant design, primarily because the intent of the device is human implantation where temperature variation was considered to be of minimal concern. However, for *in vitro* testing, large variations in temperature were both observed, and should be expected. Due to the high sensitivity of the strain gages, seemingly small fluctuations in temperature had relatively large effects on gage output—changes of one degree Celsius induced output differences on the order of 10%. To minimize this effect, initial calibration was performed after allowing the transducer to equilibrate at room temperature for 45 minutes. In addition, care was taken not to touch the transducer, as contact could induce temperature fluctuation. In an effort to further stabilize transducer temperature as much as possible, the transducers and all calibration and loading fixtures were stored in an insulated Styrofoam container containing room-temperature gel packs. These gel packs are typically used frozen to treat injuries or for cold food packing. By storing the transducers and the calibration fixtures in this container with gel packs, temperature could equilibrate over long periods of time. The transducer and fixture were then removed using insulated gloves, tested, and replaced within 15 minutes—minimizing room-induced temperature fluctuations. The practice of keeping the metal fixtures in the same storage condition further helped stabilize temperature, as they are large heat sinks and take significant time to equilibrate to room temperature. While these steps do not entirely eliminate temperature fluctuations, they have been shown to reduce them drastically, as drift over time within a run dropped to less than 1% (from a high of 10%).

The original bridge circuits included operational amplifiers on the output voltage. While this step will increase resolution and reduce noise of the measured signal, it is clearly impractical in the implanted device as space and power consumption are critical concerns. After some initial testing using these amplifiers, they were removed from the circuitry for trial testing. Resolution was acceptable with the 12-bit A/D card that was

being used for data acquisition (National Instruments, Austin, TX), and noise was small compared to drift (20-40% of drift magnitude). Circuit redesign, as described previously, was done without the amplifiers—not only was drift substantially improved, as mentioned earlier, but the hysteresis effect was gone as well. The cause of this hysteresis is unclear as it was only on certain channels, and not consistently on any one bridge circuit.

With the hysteresis effect eliminated and drift characterized, force response was investigated. Each transducer was individually loaded to approximately 100 Newtons (N) using a calibrated load cell (Omega Engineering, Santa Ana, CA) and a manual stepping load fixture. As previously observed, several channels did not exhibit the expected linear correlation between load and gage output, but this phenomenon was only observed in transducers 3 and 4—the transducers that had the strain gages mounted at a more interior position that FEA had suggested would be less sensitive. Force response data is shown in Figure 3.2. It is possible that the 100 N applied load was too small to elicit a response, since it is only 12% of the minimum load used in FEA modeling. Nonetheless, it was decided that telemetry work, calibration and feasibility testing should proceed with transducers 1 and 2 only, since their functionality was established, and at the bare-minimum attempting to move forward with both gage mounting configurations would require duplicate and parallel paths.

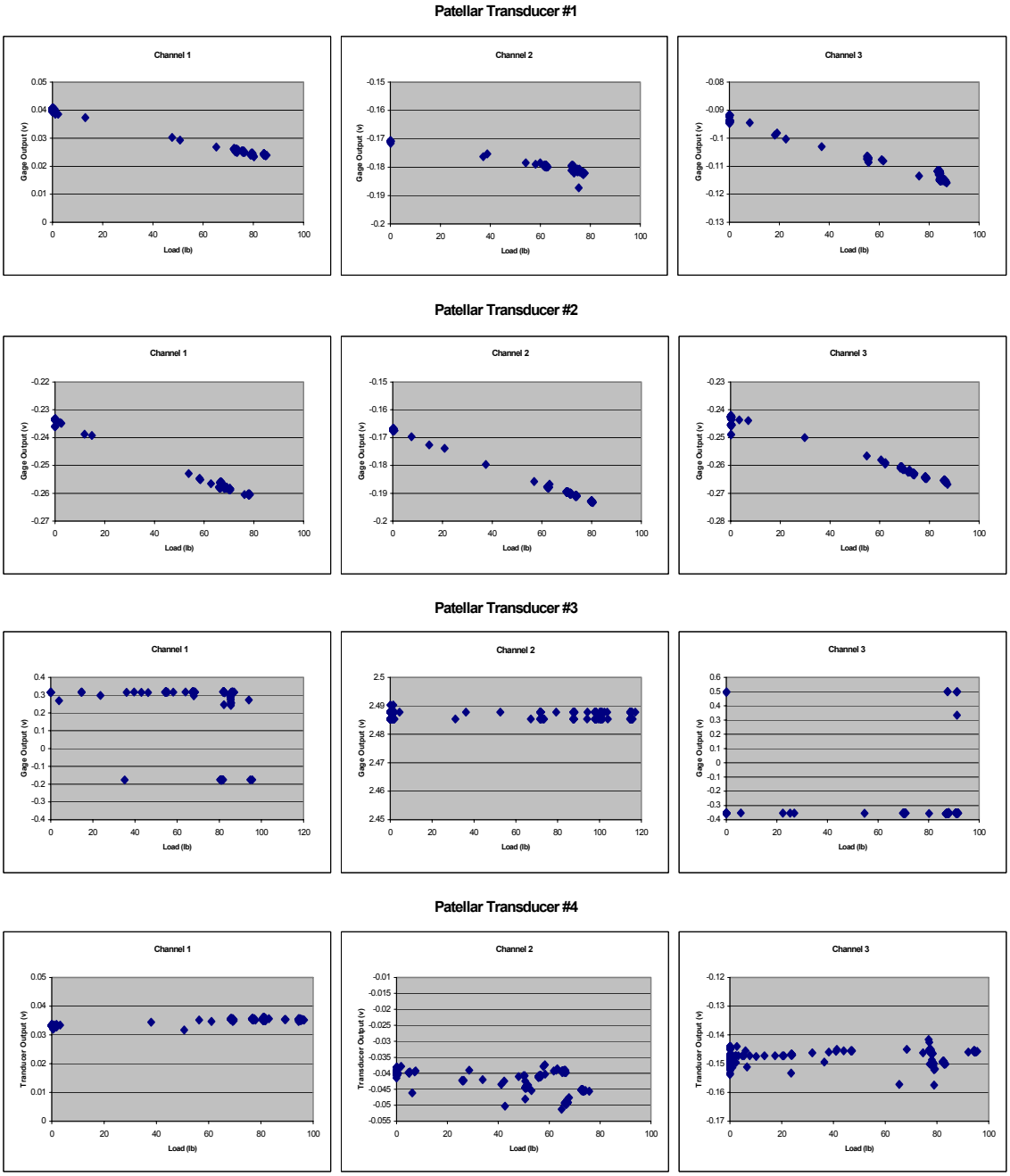


Figure 3.2: Force response data for all four transducers. The expectation is a linear relationship between the y-axis (transducer gage output) and the x-axis (applied load).

### 3.2 System Configuration for Calibration and Feasibility Testing

Several methods of signal transduction and data acquisition were utilized over the course of this project. Initial transducer testing was performed with both the amplified Wheatstone bridge circuit and the Colpitz-based transmitter. As previously mentioned, the bridge circuit was subject to drift and the amplification was impractical as a final design. The Colpitz transmitter was unpredictable in its data output, and due to the necessity to manually extract data from the signal, real-time data monitoring was nearly impossible. Work continued on the transmitter to make data acquisition user-friendly, but the focal point of the data acquisition process shifted to the bridge circuit. Significant work was undertaken to optimize the bridge circuit for minimal drift and noise while allowing for acquisition of a raw (non-amplified) signal. The results of this effort were detailed previously. Data acquisition was accomplished with a SCB-68 shielded pin-out box and LabView Virtual Instrument software (National Instruments, Austin, TX). Calibration work and investigational *in vitro* testing were performed with this configuration, and data appeared clean and reliable.

When it became clear that it was not feasible to continue work with the custom transmitter, the StrainLink system was acquired and tested. The StrainLink transmitter was interfaced with a customizable prototyping board (see Figure 2.4) to provide gage transduction and power. The protoboard could be either directly connected to the receiver, or data could be transmitted wirelessly. Both methods were utilized over the course of development. The Wheatstone bridge circuitry used in hard-wire data acquisition was duplicated on the StrainLink protoboard, with the exception that a two-wire connection was used to interface with the transducer instead of the three-wire used previously. The reason for this change is that the StrainLink circuitry design and protoboard pinout did not accommodate the three-wire design. Because the StrainLink system allows wireless data-transfer, the connection between the transducer and the bridge circuitry was significantly shorter (3 feet versus 7 feet previously), thus

minimizing the concern about capacitive effects of the wire harness. Initial testing revealed no noticeable data aberrations with the two-wire harness. The patellar transducer was connected to the protoboard into the open end of each bridge. Initially, data acquisition was accomplished both using the aforementioned NI system by taking the bridge voltages off of the protoboard, and using the MicroStrain receiver through an RS-232 port. Both signals were acquired in LabView simultaneously. After sufficient data was taken to show equivalence in data acquisition methods and acceptable calibration using the MicroStrain system, the pin-out board was removed and all data was acquired exclusively using the wireless system. The wireless data-transfer setup is shown in Figure 3.3, with the StrainLink protoboard wiring shown in detail in Figure 3.4.

Figure 3.3: Wireless data acquisition system with StrainLink instrumentation.

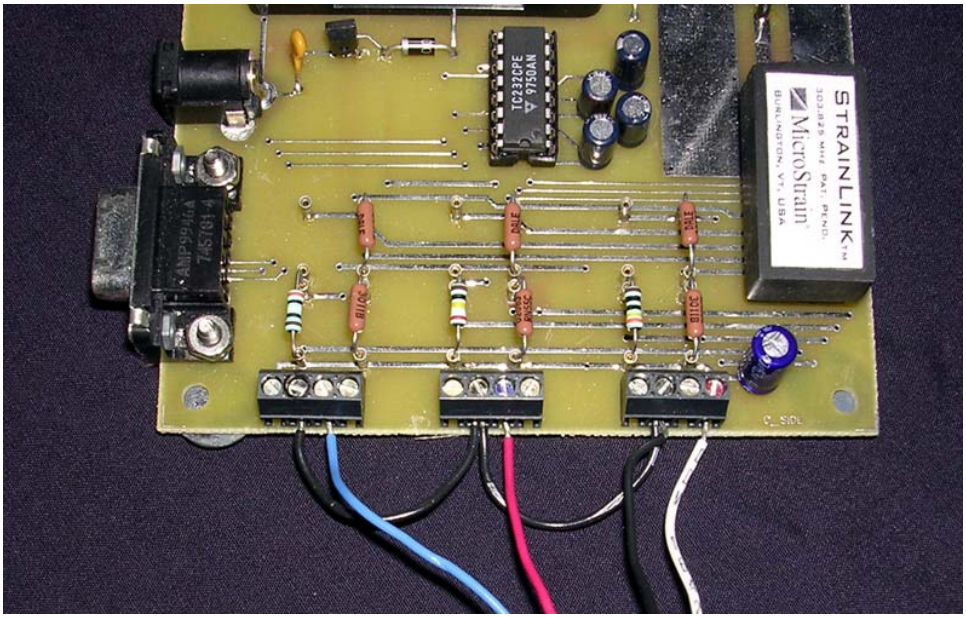


Figure 3.4: Wiring connection between the patellar transducer and StrainLink.

Final calibration data was obtained for both transducer 1 and 2 using both the wireless digital system and the wired A/D system. Several LabView routines were used throughout the development process— the routines for acquiring data with two simultaneous systems, and for acquiring data with the wireless system alone are included as appendices. Feasibility testing was performed with both transducers, the wireless acquisition system, and LabView. The StrainLink transmitter was powered using a 9-volt battery. Excitation voltage is controlled at 2.5 volts by the StrainLink chip set.

# Chapter 4

## TRANSDUCER CALIBRATION

The intended use of the telemetric patella is to measure force in three dimensions. This requires conditioning the strain gage output data to equate it to a force vector with magnitude and direction. To do this, the device must be calibrated using known loads. In addition, a coordinate system must be defined around the device's geometry so that the direction of the force can be resolved. A standard rectangular coordinate system was chosen to be the reference system for calibration. For prototype load testing it is recognized that there are advantages of using a spherical coordinate system, which is simply calculated from the rectangular coordinates described here. The z-axis is chosen as the normal vector to the patella, the x-axis is the vertical side-loading vector, and the y-axis is the lateral side-loading vector (Figure 4.1). For the spherical coordinate system, $\varphi$ is the angle from the z-axis to the force magnitude vector and $\theta$ is the angle between the y-axis and the projection of the magnitude vector in the xy-plane.

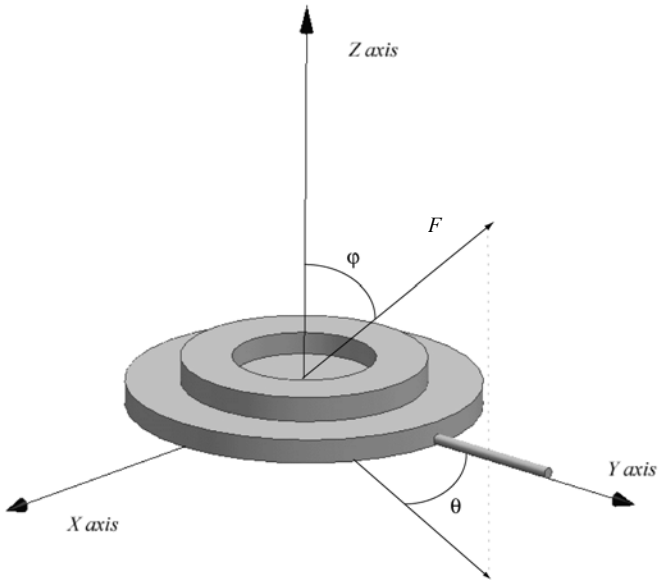


Figure 4.1: Load axis definition for the patellar transducer.

**4.1 Calibration Theory**

Calibration of the patellar transducer was significantly complicated by the complex geometry of the metal backing plate, as well as the planar nature of the transducer. The configuration of the device made it impossible to directly relate the measured strain to an applied load in three dimensions. Instead, signal processing protocols developed by Bergman et al [16] were used to relate the three strain measurements with the applied three-dimensional load. This matrix method minimized cross-talk effects that typically exist between neighboring gages, allowing for a less precise mechanical design and the ability to process loading data using fewer gages. This method relies on the fact that each gage is affected to some degree by any load that is applied to the device. By applying loads with known magnitude and direction, the measured strain is related back to these known conditions and is used to generate a matrix of calibration constants. The device is loaded along the axes of an orthogonal coordinate system in one dimension at a time, and

the output from all three gages is recorded. After repeating for all three loading axes, a matrix of scaling constants is assembled that equates the load along each orthogonal direction with the output of each strain gage. Using this system, the three-dimensional loading condition, F, takes the form:

$$F = \begin{bmatrix} f_x \\ f_y \\ f_z \end{bmatrix} \tag{E4.1}$$

where $f_x$, $f_y$ and $f_z$ are the magnitude in the orthogonal directions. Strain gage output, $S_1$, $S_2$ and $S_3$, are then equated to these applied loads as:

$$\begin{aligned} F_x &= M_{11}S_1 + M_{12}S_2 + M_{13}S_3 \\ F_y &= M_{21}S_1 + M_{22}S_2 + M_{23}S_3 \\ F_z &= M_{31}S_1 + M_{32}S_2 + M_{33}S_3 \end{aligned} \tag{E4.2}$$

or, by inverting these equations, each gage output can be equated to all three load directions:

$$\begin{aligned} S_1 &= C_{11}F_x + C_{12}F_y + C_{13}F_z \\ S_2 &= C_{21}F_x + C_{22}F_y + C_{23}F_z \\ S_3 &= C_{31}F_x + C_{32}F_y + C_{33}F_z \end{aligned} \tag{E4.3}$$

Ideally, this method is utilized by applying load in one direction at a time, giving a direct relationship between the applied load and each gage's output. After acquiring all of the "C" values, that matrix is then inverted back to the "M"-matrix, which can then be used to identify any unknown applied load given three strain outputs.

### 4.2 Methods

Prototype calibration was performed at the Orthopaedic Biomechanics lab at the University of Colorado Health Sciences Center using an Instron model 1321 load frame

and model 8500 controller. Loads applied with the Instron were quantified with an AMTI load cell (Advanced Medical Technologies Inc, Watertown, MA), and measured with LabView virtual instrument software (National Instruments, Austin, TX). Two primary signal processing / data acquisition systems were used in calibration testing: a hard-wired system in which the transducer was directly connected to an A/D data acquisition system (National Instruments); and a wireless system in which there was no direct connection between the transducer and the DAS (MicroStrain, Inc.). The resistance change in each strain gage was resolved using a ¼ active arm Wheatstone bridge circuit. The active arm was constructed with 1% tolerance metal foil resistors, matched to the unloaded resistance of each gage of each transducer (280-340 ohm). The balance arm of the bridge was constructed with 3.00 kOhm 0.1% tolerance resistors, in an effort to minimize current in the transducer, and thus minimize self-heating. Potential was acquired using a 12-bit A/D card (National Instruments) and appropriate pin-out board. The bridge circuits were excited with 5.0V, and data was acquired at 10 Hz. Hardware amplification was not used, as this luxury would not be possible in a final, implantable design. Final calibration runs were performed using the StrainLink (MicroStrain Inc.) data transfer system. The transducer was connected directly to the StrainLink transmitter circuit, while the receiver communicated with LabView via the RS-232 port.

The Instron used for calibration was only capable of loading vertically, requiring the transducer to be repositioned so the incident force ran along the axis of interest. For the normal loading condition ($f_z$), this was easily accomplished, and $C_{13}$, $C_{23}$ and $C_{33}$ (from Equation E4.3) were rapidly obtained. For the side loading conditions ($f_x$ and $f_y$), the positional restrictions of the Instron meant that the transducer would need to be held in a fixture in a vertical orientation such that the desired incident vector corresponded with the Instron loading axis. To accomplish this, an aluminum fixture was designed to seat the transducer from behind, as would be the case in knee implantation, and load the

transducer along the z-axis using a calibrated load cell (Omega Engineering, Santa Ana, CA) and a specially designed steel load cap. The articular surface of the load cap was designed to mimic the intended design of the polyethylene cap, so that load transfer would be the same for the calibration procedure as for actual use. Material differences were not taken into account. The fixture, patellar transducer, load cap and Instron are shown in Figures 4.2 and 4.4.

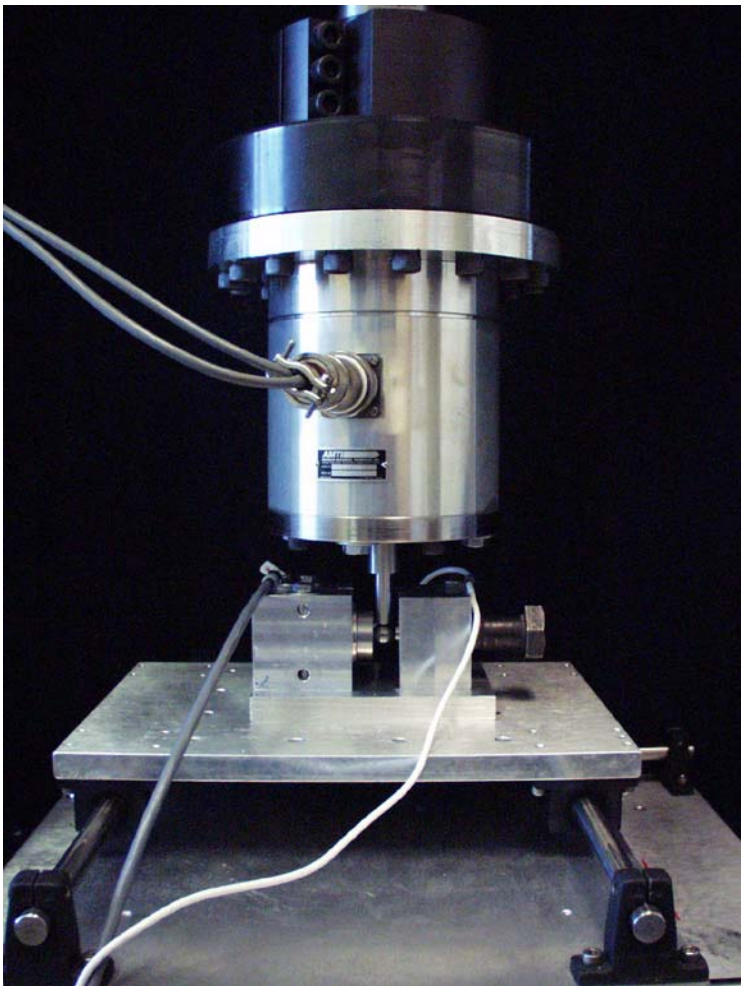

Figure 4.2: Instron 1321 with calibration fixture, transducer and load cap.

The influence of the stabilizing normal load was calculated and subtracted from the matrix calculations for the $f_x$ and $f_y$ side-loading forces. This was done using the values for $C_{13}$, $C_{23}$ and $C_{33}$ that were previously determined, and the known $f_z$ stabilizing load applied through the Omega load cell. For example, for $f_x$, the constants $C_{n1}$ were calculated with the following equation, where $f_z$ is measured and $C_{n3}$ are previously determined:

$$\begin{aligned} S_1 &= C_{11}F_x + C_{13}F_z \\ S_2 &= C_{21}F_x + C_{23}F_z \\ S_3 &= C_{31}F_x + C_{33}F_z \end{aligned} \tag{E4.4}$$

For each calibration loading cycle, a data file was created by LabView that included the Instron load, the three gage responses, and the Omega load cell output (when necessary). This data was input into Matlab (The Math Works Inc, Natick, MA) and evaluated using the appended calibration program. This program utilizes the least mean squares method to find a linear approximation for each of the three strain gage outputs versus $f_z$. To eliminate temperature effects, the bias offset (intercept of the linear approximation) is subtracted. This data was then used to compute the matrix constants $C_{13}$, $C_{23}$ and $C_{33}$, as described in Equation E4.3. For the side-loading conditions, the linear approximation was used along with the matrix constants for normal loading and the applied normal load (from the Omega load cell) to calculate $C_{11}$, $C_{21}$, $C_{31,}$ $C_{12,}$ $C_{22}$ and $C_{32}$. The resulting matrix was then inverted to give the calibration matrix, M. Each calibration data set was then reintroduced, using the M matrix to calculate the applied force—which was then compared to the known applied load. Three replicate calibration routines were performed with transducer 1, and data was analyzed as described.

### 4.3 Results and a New Method

Each individual calibration run yielded calculated force vectors that seemed reasonable compared to the input force, and error values were acceptably low. Calibration loading data for the side-loading method is shown in Appendix A. However, the M matrices for the three replicates appeared substantially different (see Table 4.1). To check the robustness of the calibration method, data from the replicate calibration routines were introduced to each of the M-matrices—for example, the normal load data set from the second calibration run was evaluated using the M-matrix from the first and third calibration runs—the results from this analysis were highly variable. In most cases, the calculated force vectors no longer coincided with the applied load (Figure 4.3), indicating that a calibration was only valid for the data used to obtain it—or more accurately, that the calibration routine was invalid. To further test this observation, calibration data from the first phase of the project were reevaluated. Once again, the calculated force for the homogeneous data matched up well with the applied load, but any allogeneous data applied to a given M matrix resulted in variant force curves.

| | | | |
|---|---|---|---|
| | 6207 | 36864 | 17502 |
| $M_1$ | 33827 | -32663 | -455 |
| | -16191 | -32364 | 58057 |
| | 2374 | 41499 | 21425 |
| $M_2$ | 43880 | -40356 | -6356 |
| | -7106 | -56080 | 54563 |
| | 8047 | 45720 | 12468 |
| $M_3$ | 35613 | -34831 | -3597 |
| | -11943 | -36519 | 42138 |

Table 4.1: M-matrices from replicate calibration routines (original method) for transducer #1.

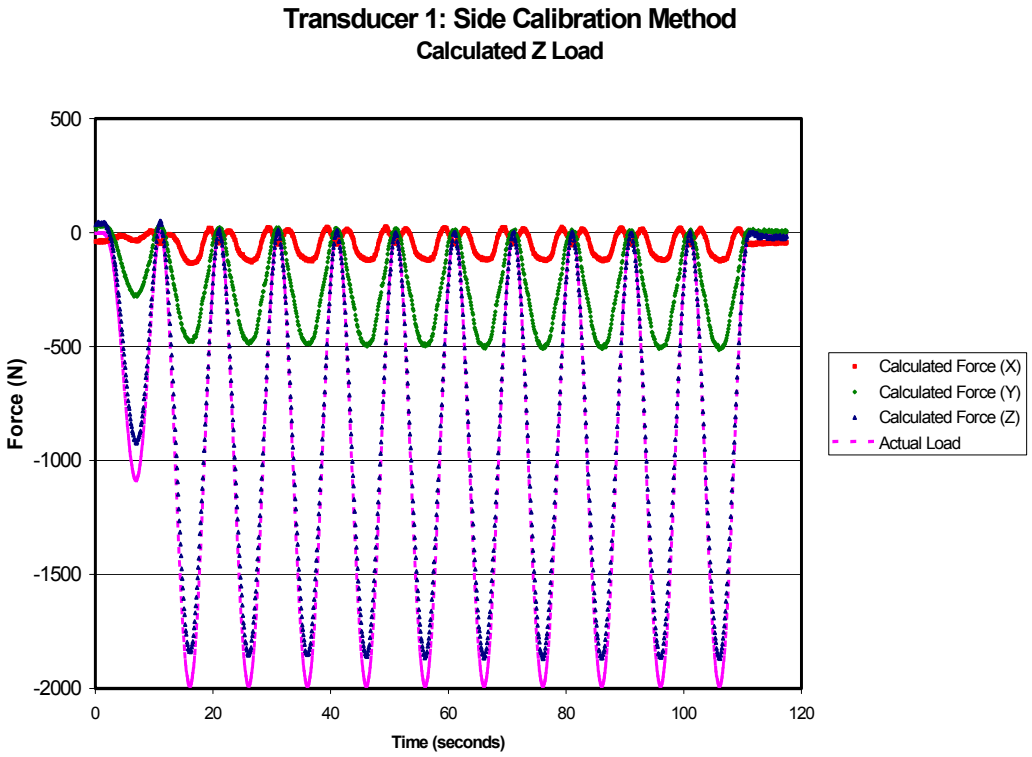


Figure 4.3: Calibration check with normal-load data set from run 2 and the M-matrix from run 1.

Further analysis of the strain gage output from the three replicate calibrations indicates a high degree of variability in the side-loading data sets after the fixed normal load had been removed. One likely explanation for this involves the way in which side loads were applied. Due to the geometry of the transducer, side loads could not be applied directly along the axis, but instead were applied to the loading cap, approximately 0.75 inches in front of the transducer plane, as shown in Figure 4.4. As a result, loading caused the load cap to bend down in relation to the load cell, creating a moment on the transducer and adding unwanted forces to the calibration cycle. In addition, the friction between the load cap and load cell caused the downward deflection to be discontinuous,

creating jumps in the calibration file. Efforts to relieve this friction accelerated the deflection, causing the moment to be worse. It became obvious that attempts to side-load the device would be extremely difficult given the loading instrumentation available, and that an alternative approach for calibration would be needed.

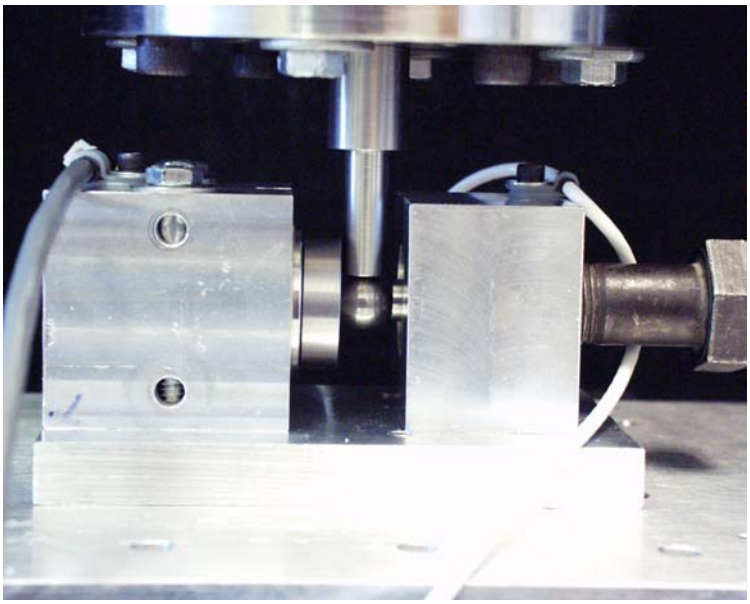

Figure 4.4: Profile of side-loading calibration method.

In an effort to eliminate side-loading, the orthogonal coordinate system was rotated out of the plane by 35.5 degrees, so that a force normal to the transducer was equi-angle from each axis of the transformed coordinate system, as in Figure 4.5. Consider a unit cube resting on the x-y plane, with the x, y and z axes representing three of the cube's sides. The diagonal of a face is $\sqrt{2}$, making the length between opposite corners of the cube $\sqrt{3}$. The vector that this value represents, extending from the origin to the point on the cube furthest from the origin, is then 54.74 degrees from each axis ($\tan^{-1}[\sqrt{2}/1]$). To rotate the entire cube such that the diagonal vector is perpendicular to the x-y plane, each

coordinate axis must then be 35.26 degrees above the plane. Due to manufacturing tolerances, a new test fixture was fabricated that mounted the transducer at 54.5 degrees from horizontal, so when the Instron loading fixture loaded the device from vertical, the load was 35.5 degrees above the plane. The transducer was then rotated within the fixture at 120 degree intervals to account for the three orthogonal arms of the coordinate system. The test fixture is diagrammed in Figure 4.6.

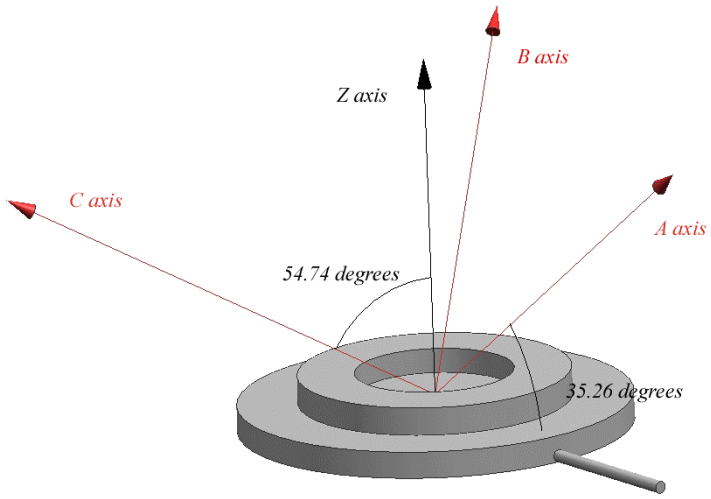


Figure 4.5: Offset coordinate system versus transducer plane and normal vector

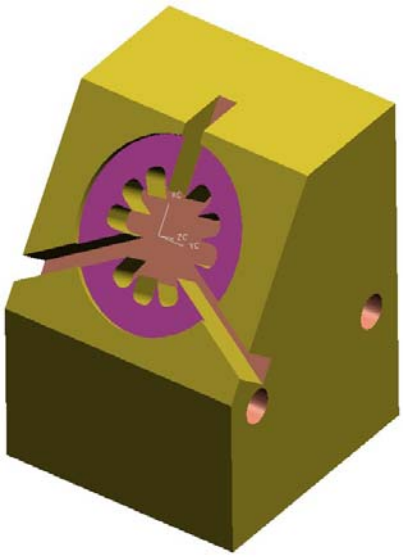

Figure 4.6: Offset calibration fixture.

In an effort to ensure that the calibration load was applied at the correct incident angle and projected through the center of the transducer, a special loading cap was fabricated from stainless steel that was beveled at 35.5 degrees. A special loading arm for the Instron fixture was designed to minimize flexion, and to point load the loading cap. These steps help ensure that the applied load extends through the center of the transducer, and when the calibration procedure is complete (all three positions), a near-orthogonal coordinate system is created that originates at the center point of the transducer. The fact that the fixtures were fabricated at 35.5 degrees ± 0.2 degrees introduces some error and lack of orthogonality to this calibration set-up. Analysis of the data from the first several calibration cycles yielded an error in measurement of 1.5-2.5%, indicating that any error introduced through inaccuracies in the machining of the fixture were not causing gross calibration error. The offset calibration setup is shown in Figure 4.7.

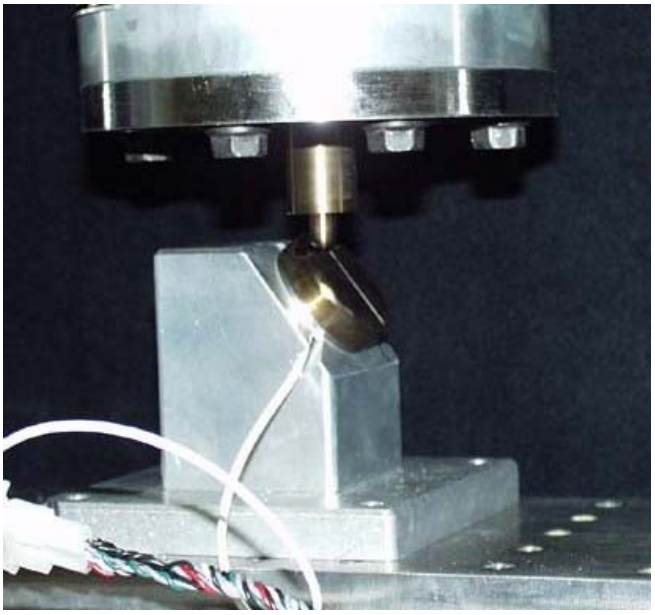

Figure 4.7: Calibration setup for the offset coordinate axes.

The axes of the new coordinate system are termed a, b, and c, and the three dimensional loading takes the form F', defined as:

$$F' = \begin{bmatrix} f_a \\ f_b \\ f_c \end{bmatrix} \tag{E4.5}$$

where $f_a$, $f_b$ and $f_c$ are the magnitude in the orthogonal directions, and are defined and calculated similarly to equations E4.2 and E4.3. Using simple geometric relationships, the forces along the a,b and c axes relate back to the x, y, z axes as described below:

$$\begin{aligned} F_Z &= (F_A + F_B + F_C)\cos 54.5^o \\ F_Y &= (F_A \cos 35.5^o) - (F_B \cos 35.5^o + F_C \cos 35.5^o)\cos 60^o \\ F_X &= (F_B \cos 35.5^o)\cos 30^o - (F_C \cos 35.5^o)\cos 30^o \end{aligned} \tag{E4.6}$$

Similarly, the measured force magnitude F, and the direction angles $\varphi$ and $\theta$ are obtained from equations E4.7:

$$F_m = \sqrt{\left(F_A{}^2 + F_B{}^2 + F_C{}^2\right)}$$
$$\varphi = \cos^{-1}\left(\frac{F_Z}{F_m}\right) = \cos^{-1}\left(\frac{(F_A + F_B + F_C)\cos 54.5^o}{F_m}\right) \qquad \text{(E4.7)}$$
$$\theta = \tan^{-1}\left(\frac{F_X}{F_Y}\right) = \tan^{-1}\left(\frac{(F_B \cos 35.5^o)\cos 30^o - (F_C \cos 35.5^o)\cos 30^o}{(F_A \cos 35.5^o) - (F_B \cos 35.5^o + F_C \cos 35.5^o)\cos 60^o}\right)$$

The results of this modified calibration system exhibit the same level of noise (error) as the normal loading condition from the original calibration method (on the order of 1.5%), but the error is similar for all three load directions, while it spiked to 5-7% for the side loading conditions in the original system. Calibration error for Patella 1 using both systems is shown in Tables 4.2 and 4.3. The substantial difference in the two calibration methods is seen with replicate calibration routines, and with test loads. Unlike the previous calibration routine, the M-matrices over replicate calibrations are comparable in value, as shown in Tables 4.4 and 4.5. Introduction of a calibration data set from the first replicate into the M-matrix of the second replicate (and vise-versa) yielded accurate force profiles. A third test of the robustness of the calibration method involved the application of a test load normal to the transducer—along the z-axis. This test load was completely independent of all calibration data sets, and was along a different axis. As shown in Figure 4.8, the calculated force is comparable to the actual force. There is still some cross-talk exhibited between the x, y, and z axes, most likely due to measurement noise and non-linearities in the calibration data. The output drift observed in Figure 4.8 is 4.7% of the measured force magnitude over the course of the 100 second load cycle. This drift is greater than the preferred value of less than 1%, but as described in Chapter 6, it is known to be caused by temperature sensitivity of the device and is not

unique to the calibration procedure. Calibration load profiles for patellar transducer 2 using the offset calibration procedure are presented in Appendix B.

| | Run 1 | Run 2 | Run 3 |
|---|---|---|---|
| X error | 5.0% | 6.0% | 5.0% |
| Y error | 6.0% | 7.5% | 5.0% |
| Z error | 2.0% | 2.5% | 1.3% |

Table 4.2: Calibration error for Patella 1 using the side-loading method.

| | Run 1 | Run 2 |
|---|---|---|
| A error | 1.5% | 1.0% |
| B error | 2.0% | 1.5% |
| C error | 2.0% | 1.5% |

Table 4.3: Calibration error for Patella 1 using the offset-axis method.

| | | | |
|---|---|---|---|
| | -1804 | 38398 | 10651 |
| $M_1$ | 34046 | 21739 | -4527 |
| | 7108 | -20880 | 41127 |
| | -1967 | 39057 | 10839 |
| $M_2$ | 34115 | 22633 | -4071 |
| | 6669 | -21156 | 40738 |

Table 4.4: M-matrices for Patella 1 from replicate calibration routines using the offset-axis method.

| | | | |
|---|---|---|---|
| $M_1$ | 19382 | 29187 | -8704 |
| | 23192 | -9883 | 13559 |
| | -8187 | 12660 | 18650 |
| $M_2$ | 20088 | 29328 | -9187 |
| | 23515 | -10094 | 13050 |
| | -8093 | 12786 | 18739 |

Table 4.5: M-matrices for Patella 2 from replicate calibration routines using the offset-axis method.

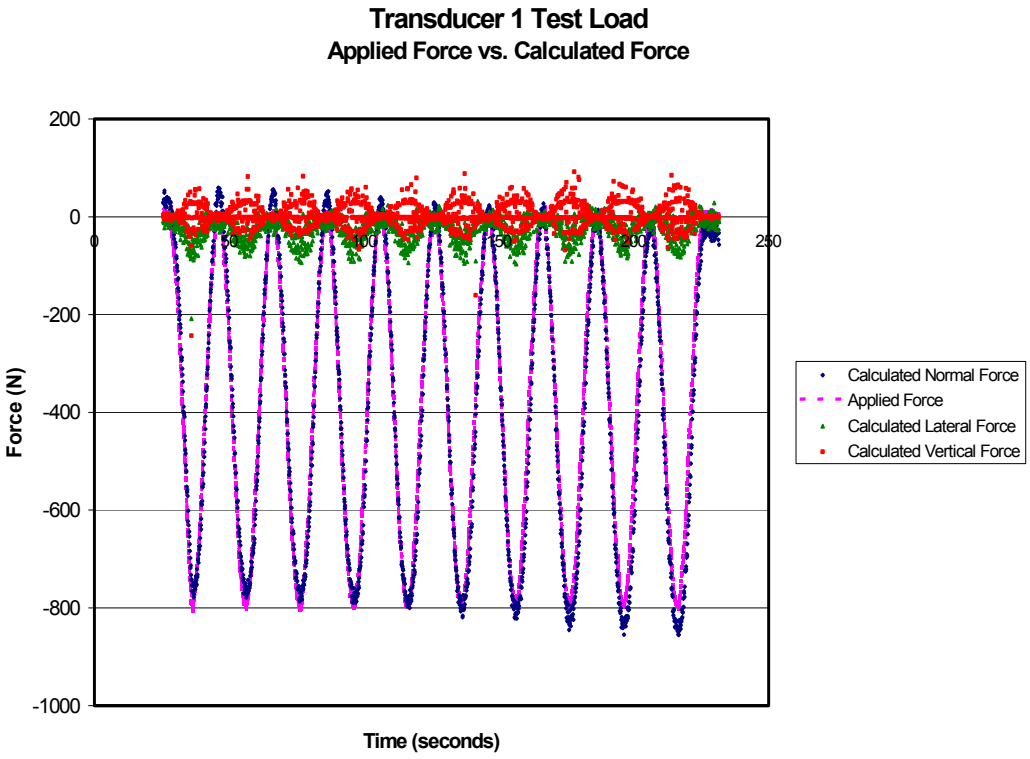


Figure 4.8: Test Load using offset calibration method. Note the drift on the calculated normal force and the coupling between the calculated lateral and vertical forces and the normal force.

### 4.4 Discussion

The drift that is still observed in the data from the latest calibration procedures, as well as in the more recent feasibility tests (see Chapter 5), is likely a primary cause of the calibration errors that are still observed. Because calibration matrices are calculated using a linear approximation of the data, a systematic downward slope of the gage output data over time will bias both the slope and the intercept of this linear approximation. Further investigation of transducer drift and potential methods of correcting or eliminating it are discussed in Chapters 6 and 7. Even with the imperfections of the current calibration procedure using the offset coordinate axes, both the accuracy and the precision are greatly improved over the original method. Despite the improvements in the calibration procedure, there are still concerns regarding the long-term reproducibility of the device calibration, as well as whether this calibration is valid for incident vectors directed from outside of the cone formed by the a-b-c calibration axes. This is discussed in Chapter 7.

# Chapter 5

# FEASIBILITY TESTING

Throughout development of the telemetric knee system, several preliminary loading studies have been performed in static loading devices, and in a simulated knee joint. In addition to testing done using the Instron and the off-axis loading fixture, as described in Chapter 4, additional static loading was performed using the original side-loading calibration fixture, where the transducer is compressed between a solid metal backing and a calibrated load cell using a set screw; and a hanging free-weight system, where the transducer is set in a "floating" cage and compressed by hanging weights from the bottom. This data was useful in software development, calibration confirmation and evaluation of linear load response. The simulated knee joint was constructed in the first phase of this project, and while it does not mimic normal knee kinematics and motion, it is valuable for evaluating transducer performance for a non-normal load, as well as performance against an artificial femoral component. While these test systems were useful in process development, it is generally believed that force resolution data in a human leg specimen is necessary to fully establish proof of principle for the telemetric knee system. This section details the testing performed with human leg specimens, and analysis of transducer performance *in situ*.

## 5.1 Study Design

The original objective of human leg specimen testing was to demonstrate that the patellofemoral contact forces tracked in a reasonable fashion with increased quadriceps load and change in flexion angle from 0 to 90 degrees. The intent was to test in multiple leg specimens and establish a trend of measured force as a function of flexion angle at

multiple quadriceps loads. Due to the anticipated differences in geometry between leg specimens, the expectation was that the patellofemoral force at a given applied quadriceps load and flexion angle would be different from specimen to specimen [31, 32], making any direct comparison between specimens difficult. After assessing the availability of leg specimens and the overall goal of the telemetric knee program, the study objectives were expanded to include comparison data between two transducers and comparison between intact and artificial femoral surfaces. In addition, an I-Scan™ thin-film joint pressure measurement system (Tekscan, South Boston, MA) was used in conjunction with the patellar transducer for comparative purposes, with the understanding that the I-Scan system has its limitations in this application and cannot be considered a "standard" for comparison [33]. Two human leg specimens were used for all testing in this portion of the project. A comparison was made between the two leg specimens tested, however the kinematic differences between the two specimens predictably led to incomparable data sets. Testing was performed statically at four flexion angles (0, 30, 60 and 90 degrees), with the expectation that the patellofemoral force at 0 degrees would be negligible, and that the contact force would increase with angle. Each leg specimen was tested with an intact femur, and again with a NexGen CR femoral implant (Zimmer Inc, Warsaw, IN). The differences in measured patellofemoral force between the intact and artificial femurs were evaluated and discussed, with no preconceived expectations regarding the relationship of this data.

Patellar transducers 1 and 2 were used in this testing. The StrainLink signal processing and transceiver system was used to process the change in resistance of the three strain gages within a transducer to electrical potential, perform A/D conversion, and transmit the digital signal to computer. The digital output of each strain channel was acquired using LabView into a Microsoft Excel file for further analysis. Using Excel, the calibration matrix for the transducer was applied to the data set and the calculated patellofemoral force was determined.

Human leg specimen testing was performed at the Orthopaedic Biomechanics Laboratory at the University of Colorado Health Sciences Center (UCHSC) using a six-degree-of-freedom load application system specifically designed and developed for testing knee specimens [34]. Testing was performed with two fresh-frozen leg specimens, cut from mid-calf to mid-femur, that had been aligned for use in the loading apparatus as the result of previous UCHSC testing with the specimens. Testing was performed with quadriceps loading at 64 pounds (29 kilograms) and 104 pounds (47 kilograms), which represents approximately half of the quadriceps load a knee would experience in normal activity [35]. Leg flexion angles were 0 degrees, 30, 60 and 90 degrees. Load testing was performed statically at these angles, as the ability of the test fixture to flex a specimen under quadriceps loading was not known.

Two leg specimens (A and B) were used for this study. These specimens were used in other projects for Colorado School of Mines and UCHSC. Specimen A was first tested for this project after it had been used for knee axis alignment testing for CSM. Implantation of the patellar transducer requires excision of knee capsule tissue beyond what is done for the axis alignment testing; this tissue excision was performed specifically for this project at the time of transducer implantation. Specimen A was tested twice with transducer 1—once for pilot testing to confirm that quadriceps loading, transducer data acquisition and signal processing, and Tekscan systems were all functioning properly, and then a second time to generate the data presented in this thesis. After testing with transducer 1 and the intact femur, the specimen was tested by UCHSC for knee stability studies. This testing required further excision of the knee capsule tissue, including the anterior cruciate and posterior oblique ligaments, resulting in decreased stability of the joint. When the specimen was tested with transducer 2 the joint was noticeably less stable, and had gone through an additional freeze-thaw cycle, both of which could impact the kinematics of the patellofemoral force vector. Specimen B was first tested for this project after the knee stability testing, and while the knee joint was in

the less-stable configuration, both transducers were tested with the specimen in the same condition. After all of the aforementioned testing, the femoral articular surface was removed from both leg specimens and replaced with a NexGen femoral implant by Dr. Donald Eckhoff, MD, Professor of Orthopedics at UCHSC. All transducer testing with the artificial femoral surface was performed on the same day, with no additional freeze-thaw cycles on the specimens.

### 5.2 Transducer Test System Methods

Implantation of the patellar transducer required minor surgery on each of the leg specimens. First, the tissue on either side of the patella was cut away, and all excess fat and muscle connected to the patellar tendon and quadriceps tendon was removed. The patella was then folded back away from the femur, exposing the articular surface. A special patella clamp cutting guide used in TKA procedures was used to clamp the patella firmly and guide the saw blade while the articular surface was removed, as shown in Figure 5.1. In order to replicate normal knee geometry, care was taken to ensure that the depth of tissue removed from the patella was as close to the transducer thickness (0.375 in.) as possible. For specimen B, slightly less tissue (approximately 0.32 in.) was removed because the patella was relatively small and there was concern about leaving enough bone for transducer fixation and stability. The articular surface was removed using a Stryker 2108 SAG surgical saw (Stryker Instruments, Kalamazoo, MI), exposing a planar region of trabecular bone. To implant the patellar transducer, an ×-shaped notch was cut into the bone using an anodized steel cutting template specifically designed for this application. The template was attached to the patella using 3/8” bone screws, as shown in Figure 5.2. The notch was cut 0.2 in. deep using a rotary tool (Craftsman) and a 0.1875 in. cylindrical router bit. After the notch was cut, the template was removed and the lateral arm of the ×-shaped notch was extended out to the edge of the patella free-

hand to allow for the transducer wire to clear the bone (Figure 5.3). The patellar transducer was then snapped into place.

Figure 5.1: A patella being held with the patella clamp / cutting guide.

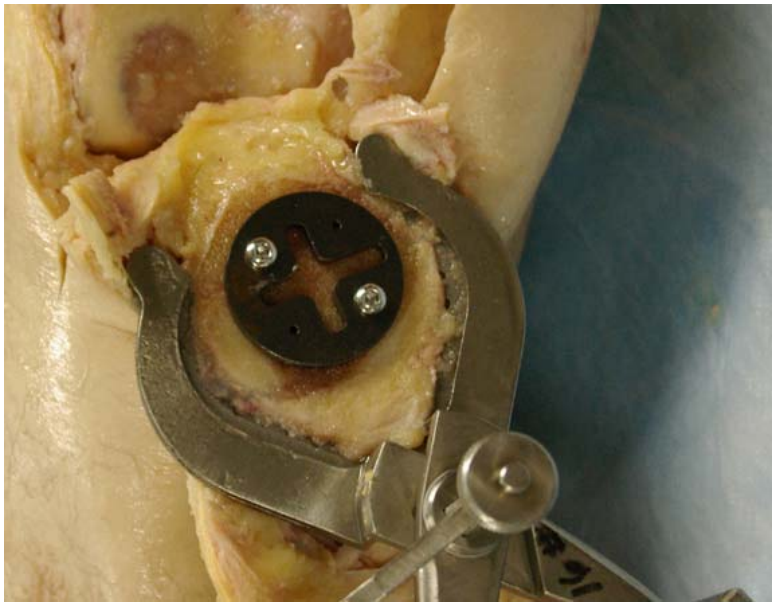

Figure 5.2: The notch-cutting template mounted to an excised patella.

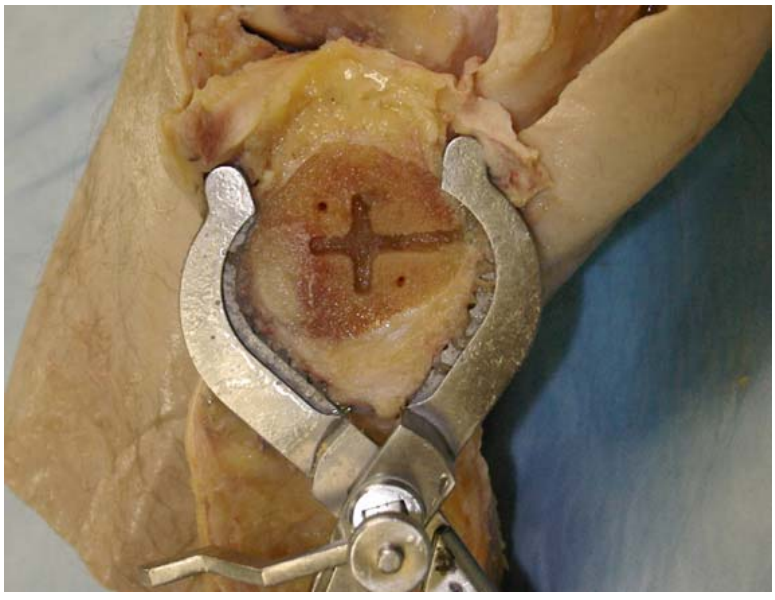

Figure 5.3: The completed notch for transducer mounting.

Application of load to the quadriceps generates a compressive patellofemoral contact force that will increase with flexion angle. A suitable attachment must be made to the remnants of the quadriceps tendon to apply this load. The tendon was saturated with RP500 adhesive (Adhesive Systems, Frankfort, IL) and inserted 2 to 3 inches into 2 in. wide tubular webbing. This connection was then stapled together with 3/8 in. P-35 industrial staples (Arrow Fastener Co, Inc., Saddle Brook, NH). This connection is shown in Figure 5.4. The attachment was allowed to dry for 20 minutes before any loading, and then was tested by firmly pulling on the webbing while holding the knee steady.

Figure 5.4: Attachment of the quadriceps tendon to the tubular webbing.

A special pulley apparatus was constructed and attached to the knee testing apparatus, allowing a weight set to hang off of the end of the structure, and re-direct the force vector along the desired line of action. The weight set was connected to the tubular webbing with 3/16 in. steel cable, which was threaded over the two pulleys of the loading apparatus (see Figure 5.5). The tendon, webbing and cable were aligned by laterally repositioning the pulleys to alleviate any contact with the knee testing apparatus.

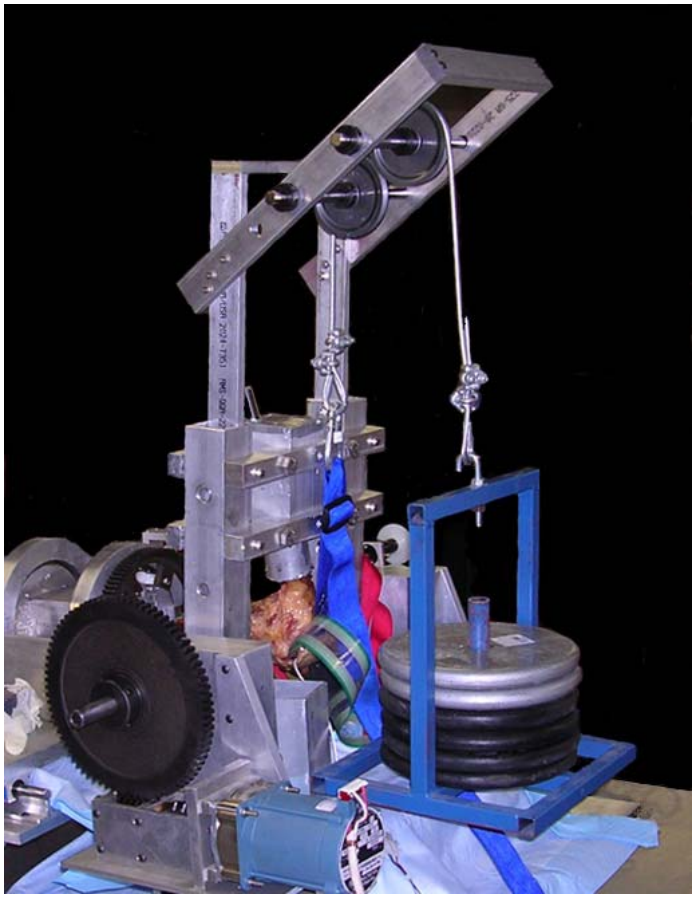

Figure 5.5: A leg specimen loaded into the knee testing apparatus. The applied load, pulley apparatus and attachment to the quadriceps are shown.

### 5.3 Transducer Testing Procedure

The pilot testing of specimen A indicated that thermal equilibrium between the leg specimen (starting at 4$^{o}$C), the transducer (starting at 22 $^{o}$C) and the room (fluctuating between 19-22 $^{o}$C) would be extremely difficult, and that it would be prudent to obtain a baseline transducer output measurement prior to each loading condition. Recall from Chapter 4 that force is calculated using the difference between the loaded strain measurement and the unloaded strain measurement. Because the transducer is highly sensitive to changes in temperature, it is important to obtain the unloaded measurement shortly before the actual measurement in unstable thermal conditions. It is recognized that this could potentially be a problem for human use, which will be addressed in Chapters 6 and 7.

Leg specimens were mounted into the knee testing apparatus as described by Bach et al [34]. The tibia is mounted horizontally in a fixture that allows for lateral and vertical motion aided by air springs. The femur is mounted in the rotating portion of the device, allowing for knee flexion. Figure 5.6 shows specimen B mounted in the fixture. The quadriceps tendon was then connected to a freely hanging weight load as described in Section 5.2. The entire system was checked for integrity and frictional contact with a load of 47 kilograms before initiating any testing. Each knee specimen was loaded at 0 degrees flexion (leg fully extended), 30 degrees, 60 degrees and 90 degrees, first with 29 kg (285 Newtons), then with 47 kg (463 Newtons). Transducer data was collected at each load condition for 10-20 seconds using the StrainLink data acquisition system, as described previously.

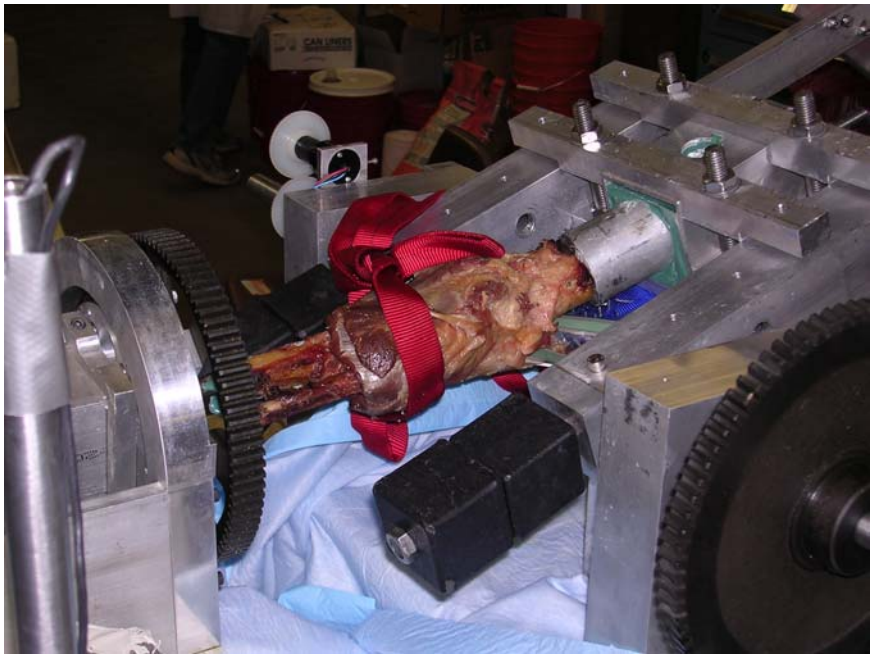

Figure 5.6: Orientation of the leg specimen in the testing apparatus. The tibia is on the left in the sliding portion of the apparatus, while the femur is in the rotating portion, on the right. The red webbing serves no functional purpose, but for orientation, it is wrapped around the tibia just inferior to the patella, which is facing downward.

Unloaded transducer data was obtained by removing the free weights from the quadriceps attachment, partially deflecting the patella so the polyethylene articular surface of the transducer was not contacting the leg, and collecting output data for 10-20 seconds. The patella was then repositioned against the femur and the free weight was reattached. Although care was taken to reposition the patella in the same orientation in all runs, it was obvious that the exact position of the patella would vary slightly from run to run. The likely impact of this small difference in patella position is that the direction of the patellofemoral force vector may vary from run to run, from knee to knee, and from transducer to transducer. The expectation is that these changes in position should not

affect the magnitude of the measured patellofemoral force, but rather the direction of the force vector.

In addition to the collection of patellar transducer data, the Tekscan thin film pressure system was used to evaluate patellofemoral force at each flexion angle and quadriceps load. After collecting the unloaded transducer data at each test condition, the Tekscan film was reinserted into the patellofemoral contact surface, the patellar orientation was realigned, and the load was reapplied. Tekscan film placement and patellar orientation were checked by evaluating the load distribution using the Tekscan software. The Tekscan system works on a pressure-pixel principle, where the film transducer is divided into a pixel field, and each pixel detects pressure at that point. Increased pressure is represented graphically as a change in color, where dark red is the maximum pressure a particular pixel can sense—the saturation point. A Tekscan pressure sample plot from specimen A is shown in Figure 5.7. The Tekscan output showed pixel saturation during many of the loading configurations, indicating that the patellofemoral force value obtained from the Tekscan would be less than the actual force. In addition, as illustrated in Figure 5.7, the contact area between the femoral condyles and the patellar transducer was not always captured in the Tekscan pixel field, indicating that the total net force was not captured. The Tekscan was incorporated into the experimental system with the intent of using the data as a standard to compare the patellar transducer calculated load value to, however the observed pixel saturation and problems with capturing the entire contact surface in the pixel field both indicated that this intended use would not be feasible. Tekscan data was still captured for all loading experiments and is presented here for discussion purposes.

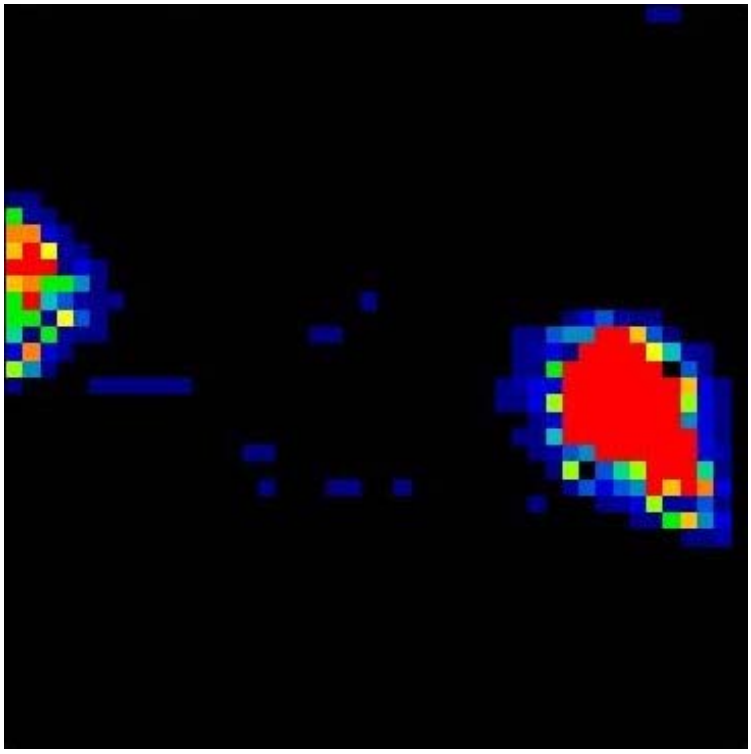

Figure 5.7: Tekscan pressure graph for specimen A (intact) at 29 kg and 60$^{o}$ flexion. Red pixels indicate saturation; the condyle on the left is only half in the pixel field, therefore the contact force is not adequately captured.

### 5.4 Results and Discussion

For each loading condition (weight and angle) a new baseline transducer output value was obtained. Data was captured at 10Hz for 10-20 seconds for each baseline value and each loading condition. The output from each gage was averaged over all values for each condition. Forces along the A, B, and C calibration axes were then calculated using the difference between the average value of the loaded transducer and the average value of the unloaded transducer. Force magnitude and direction (in spherical coordinates) were then calculated from equation E4.7. The calculated

patellofemoral contact force for each transducer in each leg specimen (both intact and NexGen) is listed in Table 5.1. Tekscan data for these conditions are listed in Table 5.2.

**Intact Femoral Surface**

| | Specimen A | | Specimen B | |
|---|---|---|---|---|
| | Patella 1 | Patella 2 | Patella 1 | Patella 2 |
| 285 N, 0° | 22 | 19 | 57 | 22 |
| 30° | 155 | 187 | 95 | 86 |
| 60° | 144 | 208 | 83 | 152 |
| 90° | 125 | 214 | 176 | 162 |
| 463 N, 0° | 36 | 10 | 24 | 13 |
| 30° | 253 | 230 | 122 | 125 |
| 60° | 244 | 386 | 112 | 229 |
| 90° | 255 | 367 | 361 | 324 |

**NexGen Artificial Femoral Surface**

| | Specimen A | | Specimen B | |
|---|---|---|---|---|
| | Patella 1 | Patella 2 | Patella 1 | Patella 2 |
| 285 N, 0° | 125 | 122 | 41 | 49 |
| 30° | 161 | 189 | 82 | 96 |
| 60° | 160 | 256 | 125 | 164 |
| 90° | 159 | 253 | 208 | 225 |
| 463 N, 0° | 162 | 148 | 56 | 28 |
| 30° | 238 | 293 | 97 | 122 |
| 60° | 255 | 418 | 187 | 251 |
| 90° | 286 | 463 | 361 | 371 |

Table 5.1: Total patellofemoral contact force magnitude, in Newtons.

**Intact Femoral Surface**

| | Specimen A | | Specimen B | |
|---|---|---|---|---|
| | Patella 1 | Patella 2 | Patella 1 | Patella 2 |
| 285 N, 0° | 0 | 0 | 18 | 62 |
| 30° | 120 | 133 | 53 | 169 |
| 60° | 151 | 102 | 160 | 160 |
| 90° | 124 | 111 | 151 | 187 |
| 463 N, 0° | 0 | 0 | 58 | 84 |
| 30° | 196 | 142 | 142 | 151 |
| 60° | 244 | 164 | 182 | 178 |
| 90° | 191 | 187 | 271 | 289 |

**NexGen Artificial Femoral Surface**

| | Specimen A | | Specimen B | |
|---|---|---|---|---|
| | Patella 1 | Patella 2 | Patella 1 | Patella 2 |
| 285 N, 0° | 0 | 18 | 22 | 18 |
| 30° | 36 | 31 | 31 | 36 |
| 60° | 40 | 40 | 40 | 36 |
| 90° | 40 | 40 | 40 | 36 |
| 463 N, 0° | 22 | 22 | 18 | 13 |
| 30° | 44 | 40 | 40 | 36 |
| 60° | 58 | 49 | 53 | 49 |
| 90° | 49 | 53 | 44 | 58 |

Table 5.2: Tekscan force readings, in Newtons.

The measured patellofemoral forces from the patellar transducers (Table 5.1) illustrate a trend of increased force with increased angle, as anticipated [11, 31]. This data is presented graphically in Figures 5.8 – 5.11. While there are individual cases of non-linear relationship between the measured patellofemoral force and flexion angle, the overall trend of the data is toward increased contact force with increased angle. The graphical data in Figures 5.8 – 5.11 show this trend similarly for a given load configuration, although the agreement in measured contact force between transducers is not what was expected. The large differences between transducer 1 and transducer 2 in

specimen A at 60 and 90 degrees can be attributed to the differences in knee stability caused by the removal of the anterior cruciate and posterior oblique ligaments between testing of transducer 1 and transducer 2. This statement is supported by the fact that the two transducers are in closer agreement with one another in specimen B—although there is still considerable discrepancy at 60 degrees in the intact specimen. The observation that the difference between the measured patellofemoral forces from the two transducers is not constant indicates that the discrepancy is not solely due to inconsistencies in the calibration procedure.

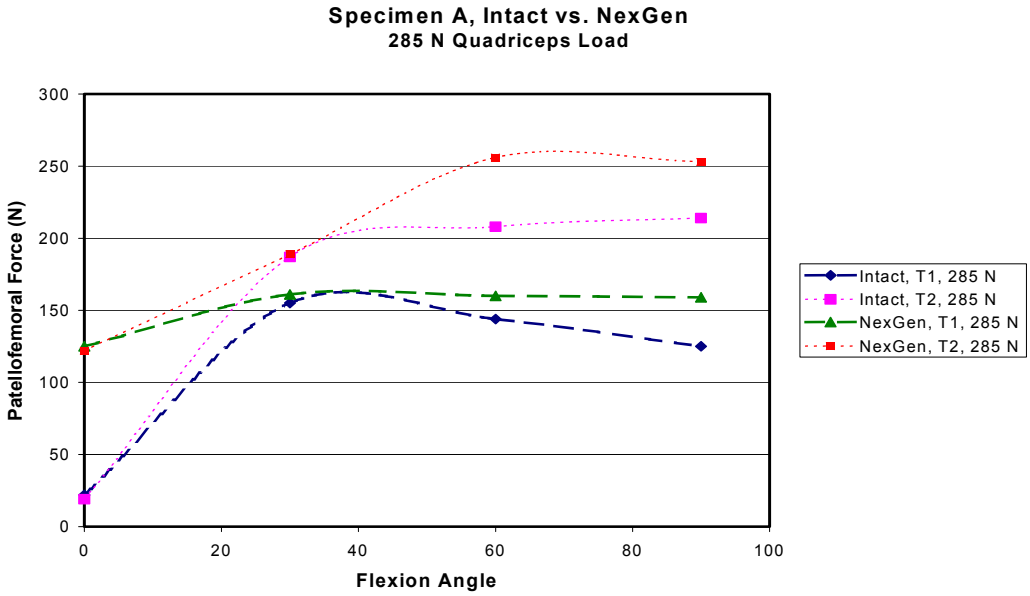


Figure 5.8: Measured patellofemoral contact force for specimen A with 285N quadriceps load.

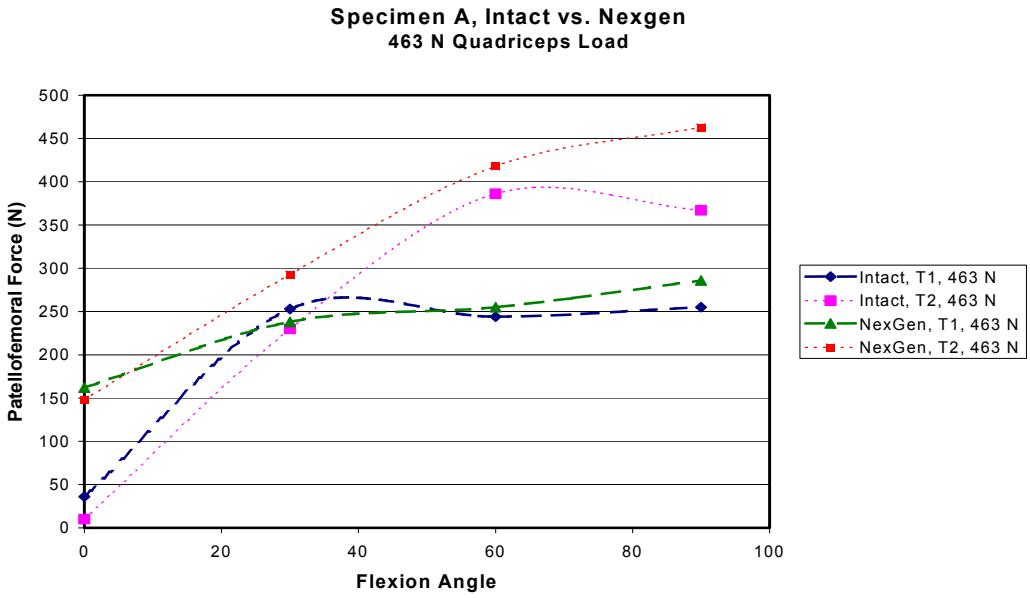


Figure 5.9: Measured patellofemoral contact force for specimen A with 463N quadriceps load.

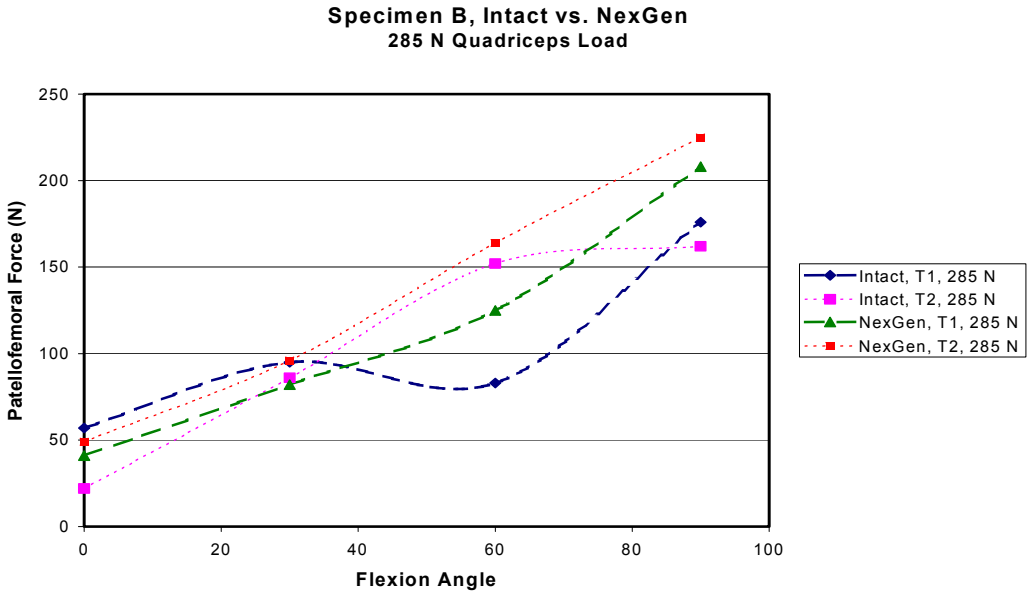


Figure 5.10: Measured patellofemoral contact force for specimen B with 285N quadriceps load.

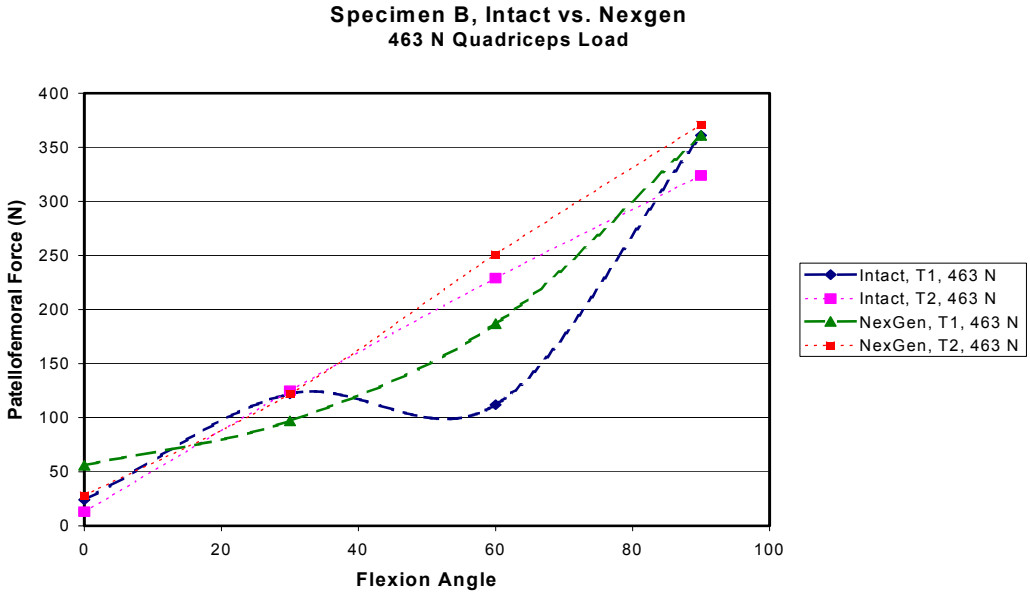


Figure 5.11: Measured patellofemoral contact force for specimen B with 463N quadriceps load.

An additional observation that can be made from the data in Figures 5.8 – 5.11 is that the measured contact force between the intact femur and the patellar transducer and the NexGen femoral component and the patellar transducer are very similar and trend much more similarly than the two transducers. The only instances where the measured forces stand out as consistently different is the fully extended (0 degrees flexion) case for specimen A. It was noted during testing that the contact force between the patellar transducer and the NexGen component was sufficiently noticeable in this specimen, while the patella barely even contacted the femur in the two intact cases. For the condition with the NexGen implant in specimen B, the patella was contacting the NexGen component with some force, but it was minimal.

As was discussed in Section 5.3, force data from the Tekscan was known to be problematic and would likely not function well as a source of comparison. Nonetheless,

analysis of the values between Table 5.1 and Table 5.2 reveal several points of discussion. Comparison of the Tekscan data to the patellar transducer data reveals two distinct data sets. The Tekscan data with the NexGen femoral implants shows very low patellofemoral force at all flexion angle and applied quadriceps loads, and shows no variation due to either flexion angle or quadriceps load. The Tekscan data for the intact femur condition does show a general increase in patellofemoral force due to quadriceps load, but displays a much higher degree of fluctuation and curvature than any of the transducer data. As discussed in Section 5.3, problems were encountered when using the I-Scan with capturing the entire contact surface in the pixel field, and with pixel saturation in the regions that were captured—both of which explain the data presented here. Tekscan has another thin-film pressure measurement system (K-Scan) designed specifically for measuring joint contact pressure and forces [33]. This system was not available at the Orthopaedic Biomechanics Laboratory at UCHSC at the time of this testing.

As mentioned previously, pilot testing with specimen A revealed that the transducer output was drifting rapidly—presumably due to lack of thermal equilibrium. In an effort to mitigate this problem for the feasibility testing, leg specimens were warmed at room temperature for 30 minutes before any work was done, and then were allowed to thermally equilibrate with the transducer for 1 hour before testing. After the transducer was supplied power and data was being transmitted, there was an additional 10-20 minute wait period before any loading was performed to allow for further equilibrium—gage output was monitored with LabView during this wait period. While it was apparent that transducer output was still drifting, it was believed that the drift was slow enough that a background transducer output point before every test point would be sufficient. While the exact cause of the unanticipated load profiles shown in Table 5.1 is difficult to determine, the instability of temperature throughout the experiment, and in particular

from the time the background output was measured to the time the loaded transducer was measured, is thought to be a primary cause of aberrant patellofemoral force data.

In an effort to establish a better estimate of the unloaded transducer baseline output at a given time point, the unloaded data for each test run was evaluated as a function of time, a sample of which is shown in Figure 5.7. This illustrates the fluctuating baseline resistance of each gage over time—a phenomenon that is now known to be the result of both inadequate temperature equilibration, and a self-heating effect that is described in detail in Section 6.3. The second-order fit baseline signal curve shown in Figure 5.12 is likely the result of the thermal imbalance of the leg, transducer and room. Self-heating effects are only seen in a small percentage of the data sets, as shown in Figure 5.13, in which the experiment was initiated before the internal gage temperature in the transducer had stabilized—which is now known to take 20-30 minutes. To estimate a more appropriate zero-load value, each zero-load output profile from each gage, for each test, was fit with a second-order polynomial as in Figure 5.12. A few of these profiles, like the example shown in Figure 5.13, can be reasonably approximated with a linear-fit, but a second-order approximation was used for all cases for consistency, with the understanding that in some cases the second-order term is negligible. The time for which each load condition was run (computed as the average over the data collection period) was then used in the polynomial equation to generate a theoretical value for zero-load output. This value was then subtracted from each measured value for a given load condition (again, computed as the average over the data collection period), and subjected to the calibration matrix for that patella. The new contact force values are shown in Table 5.3.

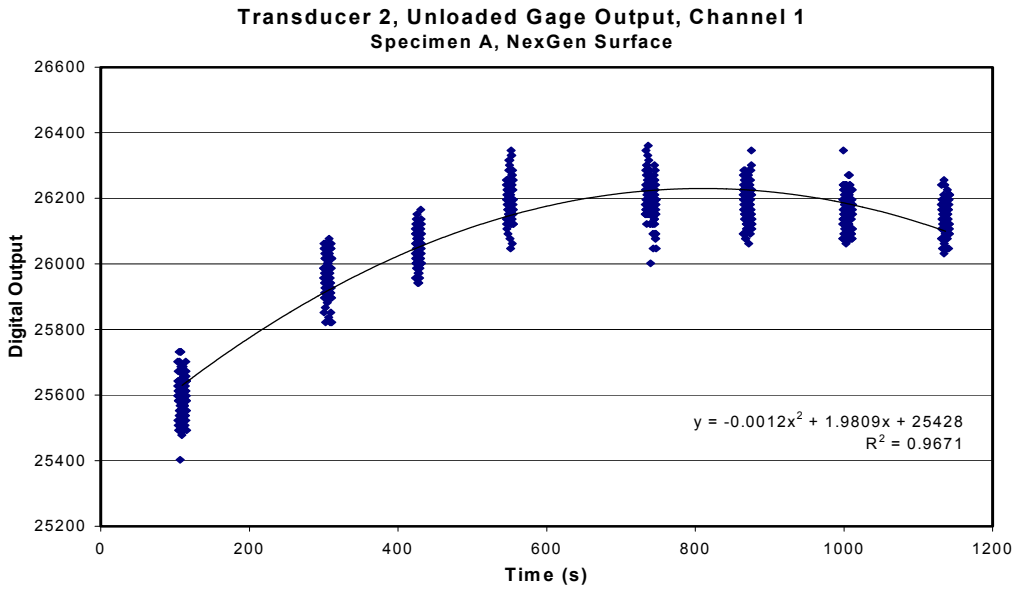


Figure 5.12: Unloaded data output from gage 1 of transducer 2 in specimen A with the NexGen femoral surface.

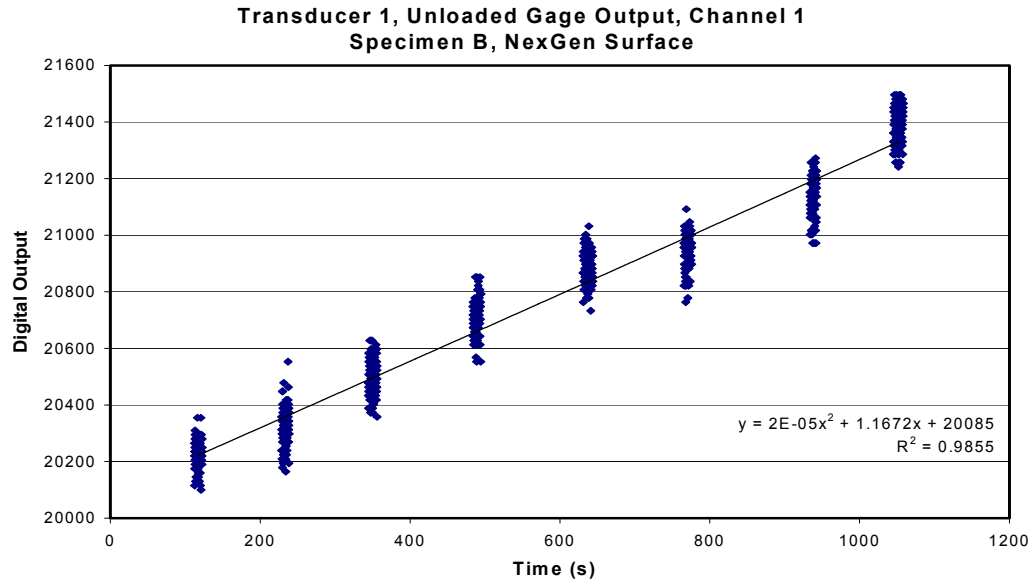


Figure 5.13: Unloaded data output from gage 1 of transducer 1 in specimen B with the NexGen femoral surface.

**Intact Femoral Surface**

| | Specimen A | | Specimen B | |
|---|---|---|---|---|
| | Patella 1 | Patella 2 | Patella 1 | Patella 2 |
| 285 N, 0° | 11 | 3 | 53 | 23 |
| 30° | 156 | 211 | 92 | 72 |
| 60° | 148 | 211 | 90 | 147 |
| 90° | 128 | 210 | 180 | 165 |
| 463 N, 0° | 20 | 7 | 25 | 69 |
| 30° | 248 | 221 | 122 | 141 |
| 60° | 256 | 389 | 107 | 247 |
| 90° | 280 | 381 | 363 | 364 |

**NexGen Artificial Femoral Surface**

| | Specimen A | | Specimen B | |
|---|---|---|---|---|
| | Patella 1 | Patella 2 | Patella 1 | Patella 2 |
| 285 N, 0° | 125 | 99 | 22 | 30 |
| 30° | 158 | 177 | 67 | 90 |
| 60° | 156 | 245 | 116 | 154 |
| 90° | 159 | 256 | 210 | 223 |
| 463 N, 0° | 169 | 148 | 34 | 29 |
| 30° | 244 | 285 | 69 | 115 |
| 60° | 282 | 415 | 159 | 240 |
| 90° | 343 | 479 | 358 | 387 |

Table 5.3: Total patellofemoral contact force magnitude, in Newtons.
Values were calculated using the ***mathematically optimized*** zero values.

The new force values shown in Table 5.3, using theoretical unloaded values to zero the transducer, do not provide any improvement from the values in Table 5.1. While there are slight differences in some of the values, the overall appearance of the data set is similar, with minimal changes in the correlation between patellofemoral force and flexion angle. In general terms, the observations made relative to the original data (measured background transducer output) still apply, with some improvement in some of the correlations, but nothing that can be mathematically substantiated. Patellofemoral force as a function of flexion angle using the mathematically optimized background transducer output values are presented graphically in Figures 5.14 – 5.17.

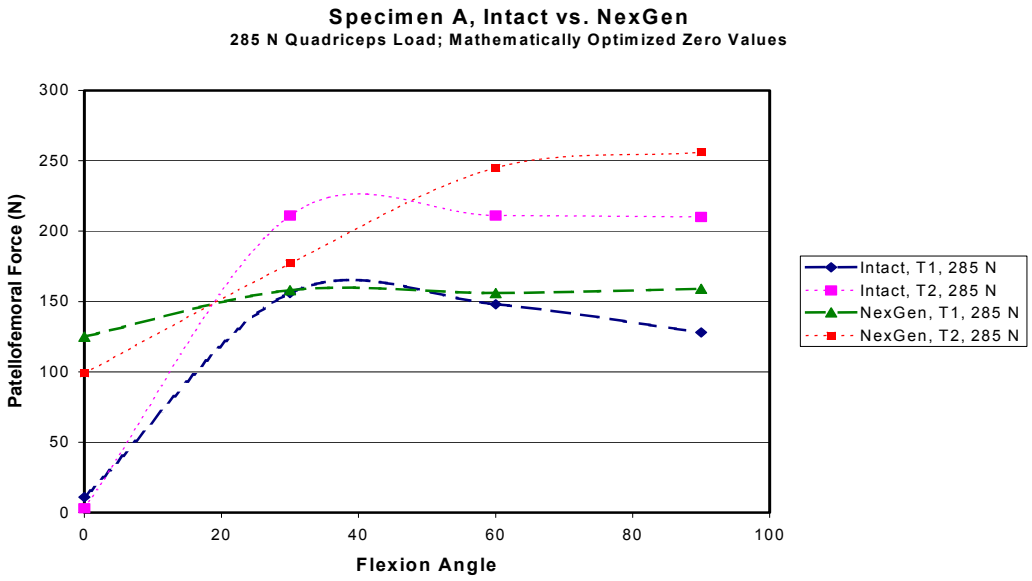


Figure 5.14: Measured patellofemoral contact force for specimen A with 285N quadriceps load using mathematically optimized zero values.

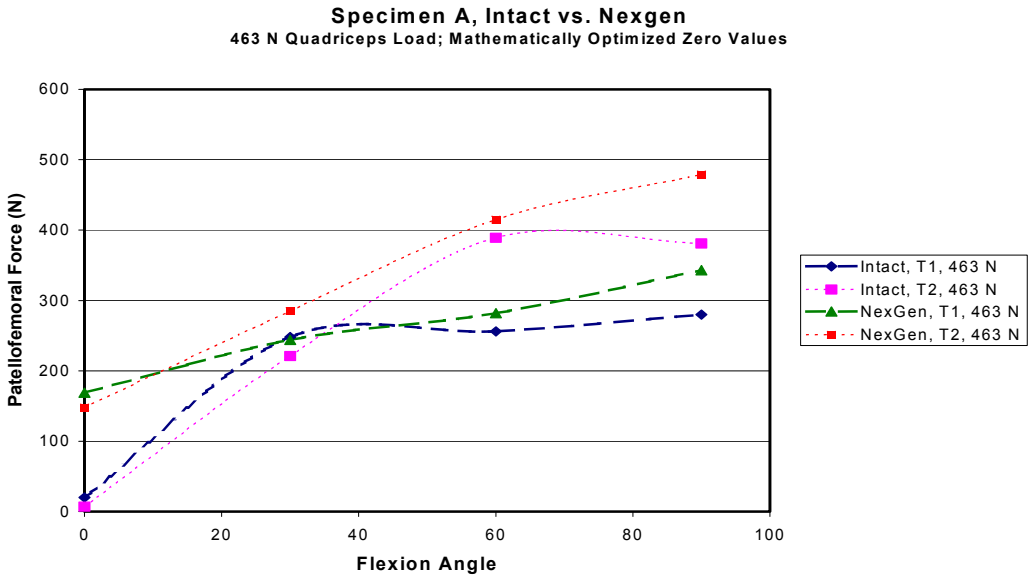


Figure 5.15: Measured patellofemoral contact force for specimen A with 463N quadriceps load using mathematically optimized zero values.

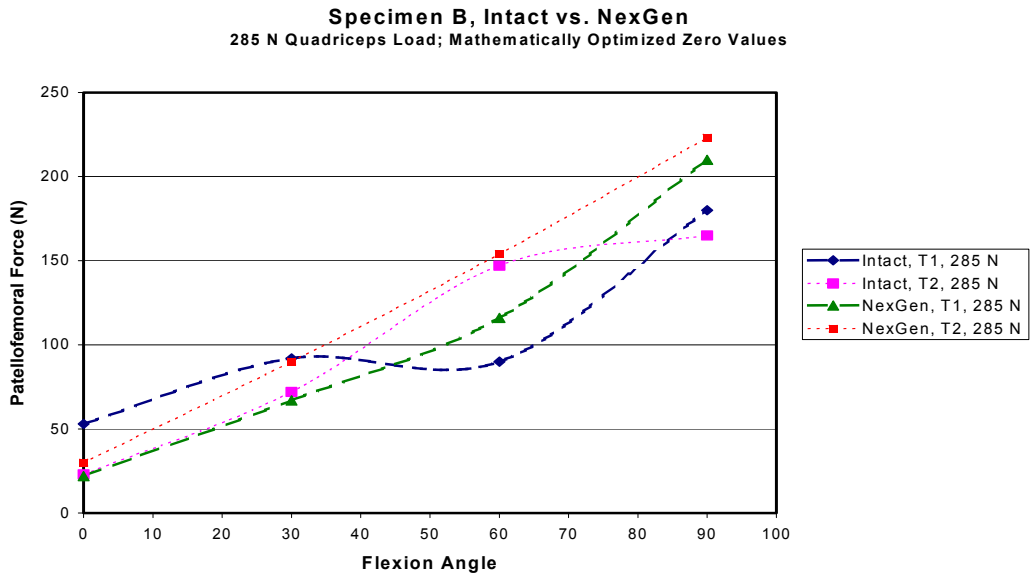


Figure 5.16: Measured patellofemoral contact force for specimen B with 285N quadriceps load using mathematically optimized zero values.

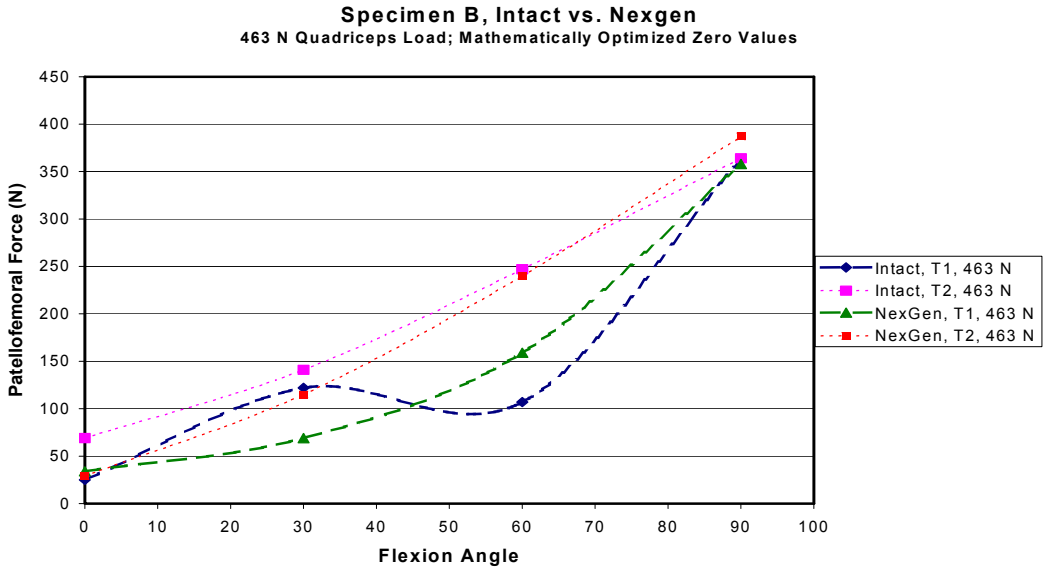


Figure 5.17: Measured patellofemoral contact force for specimen B with 463N quadriceps load using mathematically optimized zero values.

Significant discussion has been made of the magnitude of the measured contact force in these studies, and rightly so as this data was the intended output of the human leg specimen testing. However, attention must be paid to the vector direction data, as this information is key to understanding intricacies of the magnitude data. As mentioned previously and in Chapter 4, vector direction is given in spherical coordinates, as defined in Figure 4.1. The angle $\varphi$ represents the angle between the patellofemoral force vector and the z-axis. Because the z-axis is defined as coming out of the articular surface of the patella into the femur, a $\varphi$ angle of $180^{o}$ indicates a fully normal and compressive patellofemoral force vector. The angle $\theta$ is the angle between the y-axis and the projection of the patellofemoral force vector in the x-y plane. The y-axis is defined along the gage lead wire of the transducer—for this feasibility testing, the transducer was implanted with the lead wire exiting the patella laterally, meaning that for a right knee the x-axis travels inferiorly from the patella, and for a left knee it travels superiorly from the patella. Subsequently, this means that in a right knee, a positive $\theta$ represents an inferiorly oriented patellofemoral force vector, while in a left knee a positive $\theta$ represents a superiorly oriented force vector. In either knee, a $\theta$ angle with an absolute value less than 90 degrees indicates a laterally directed patellofemoral force vector, while a $\theta$ with an absolute value greater than 90 degrees (and less than 180) indicates a medially directed force vector. Specimen A was a left knee, and specimen B was a right. The measured $\varphi$ and $\theta$ angles for the patellofemoral force vectors for each transducer in each leg specimen are listed in Table 5.4.

**Intact Femoral Surface**

| | Specimen A | | | | Specimen B | | | |
|---|---|---|---|---|---|---|---|---|
| | Patella 1 | | Patella 2 | | Patella 1 | | Patella 2 | |
| | $\varphi$ | $\theta$ | $\varphi$ | $\theta$ | $\varphi$ | $\theta$ | $\varphi$ | $\theta$ |
| 285 N, 0° | 157 | -179 | 161 | 165 | 100 | -107 | 154 | -59 |
| 30° | 121 | 110 | 153 | -166 | 92 | -102 | 161 | -23 |
| 60° | 147 | 139 | 146 | -131 | 144 | 29 | 156 | -8 |
| 90° | 164 | 157 | 143 | -124 | 122 | 73 | 170 | 72 |
| 463 N, 0° | 23 | 111 | 45 | -36 | 106 | -103 | 91 | 25 |
| 30° | 120 | 112 | 153 | -177 | 114 | -112 | 160 | -37 |
| 60° | 144 | 147 | 142 | -132 | 167 | 96 | 167 | -20 |
| 90° | 154 | 167 | 137 | -127 | 129 | 75 | 168 | 103 |

**NexGen Artificial Femoral Surface**

| | Specimen A | | | | Specimen B | | | |
|---|---|---|---|---|---|---|---|---|
| | Patella 1 | | Patella 2 | | Patella 1 | | Patella 2 | |
| | $\varphi$ | $\theta$ | $\varphi$ | $\theta$ | $\varphi$ | $\theta$ | $\varphi$ | $\theta$ |
| 285 N, 0° | 112 | 148 | 151 | -171 | 127 | -129 | 165 | 34 |
| 30° | 111 | 134 | 148 | -162 | 157 | -60 | 160 | -2 |
| 60° | 127 | 143 | 146 | -132 | 164 | 64 | 176 | 23 |
| 90° | 138 | -165 | 143 | -122 | 134 | 73 | 171 | 122 |
| 463 N, 0° | 87 | 145 | 139 | -180 | 130 | -114 | 148 | 19 |
| 30° | 107 | 40 | 147 | -161 | 148 | -48 | 159 | 3 |
| 60° | 122 | 150 | 144 | -135 | 164 | 59 | 179 | 145 |
| 90° | 131 | -170 | 139 | -127 | 127 | 71 | 169 | 145 |

Table 5.4: Direction angles of the patellofemoral force vector.
$\varphi$ is the angle from the positive z-axis, 180° is a compressive force directly along the z-axis; $\theta$ is the angle of the vector projection in the x-y plane from the y-axis.

Analysis of the angle $\varphi$ shows that for a given leg specimen and transducer, the deflection of the patellofemoral force vector from the z-axis is consistent between quadriceps loads and femoral surface for a given angle. The one exception to this is specimen A with Transducer 1, where the anterior cruciate and posterior oblique ligaments were removed between testing with the intact femoral surface and testing with

the NexGen femoral surface. In fact, this vector direction data confirms the previous observation that the geometry and stability of the specimen had changed following that tissue excision. The other main observation from the $\varphi$ data is that there are large side-loading components to the patellofemoral force in most cases. Since a $\varphi$ of $180^{o}$ would indicate a purely normal force, and $90^{o}$ would be purely lateral, a vast majority of the individual measurements are in the range of 50-60% normal and 40-50% lateral.

Analysis of the $\theta$ angle provides some insight into the characteristics of the lateral components of the patellofemoral force vector. The two specimens behave differently from each other, and unlike the deflection component ($\varphi$), the positional component ($\theta$) exhibits more variation between the intact femoral surface and the NexGen femoral surface. This is intuitive, since the geometry of the natural condyles is very different from that of the NexGen condyles, and will therefore contact the spherical surface of the polyethylene dome differently. Also, the $\theta$ angle is more dependent upon the way the transducer is manual positioned relative to the femur at each loading condition than the $\varphi$ angle is. For specimen A, there is a tendency for the transducer to rotate laterally, causing the force vector to orient medially—which is indicated in Table 5.4 by $\theta$ angles with an absolute value between 90 and 180 degrees. The data also suggests that transducer 1 favors a downward deflection, while transducer 2 favors an upward deflection. This is odd, considering that the geometry of the two transducers is identical. For the intact femur case, the joint geometry changed between testing of transducers 1 and 2, which could lead to this difference in top-to-bottom in orientation, but the same trend is seen in the NexGen case (although less pronounced), where the joint geometry was the same for the two transducers. For specimen B there is more of a medial rotational trend in the intact femur case, and even distribution of medial and lateral rotation in the NexGen femur case. Again, this can be attributed to differences in geometry between the specimens and between the femoral surfaces. As in specimen A, there are consistent differences in $\theta$ between transducers 1 and 2, which is less obvious

for this specimen due to the fact that the knee joint geometry did not change between transducer testing runs.

Overall, the data from the human cadaver trials demonstrates that the patellar transducer does track the patellofemoral contact force with increased load and changes in flexion angle. Data from specimen B indicates a roughly linear relationship between patellofemoral force and flexion angle, while specimen A behaves in a more logarithmic fashion—the force increases rapidly with increased angle, and then levels off from 60 – 90 degrees flexion. These differences in the relationship between patellofemoral force and flexion angle are likely due to differences in specimen geometry. In all cases, transducer 1 and transducer 2 behave similarly to one another in a given knee configuration, although the reported force is similar in only a fraction of the conditions. This is attributed to the lack of temperature equilibrium between the leg, the transducer and the room, as well as improper adjustment for transducer self-heating effect, and insufficient control of patellar orientation relative to the femur.

Despite the many positive observations made from this study, the variability in the preceding data, coupled with the general lack of correlation between transducers, indicates that additional testing is warranted with this transducer system before feasibility can be claimed. Immediate testing needs include reproducibility testing of the two transducers under replicable conditions—this has been done in the mechanical knee assembly as described in Section 6.1, as well as in the Instron compression device (Section 6.2). Second, the drift and temperature dependence of the transducer must be fully characterized, and possible solutions and/or methods of circumvention should be defined—this work is detailed in Sections 6.3, 6.4 and 7.1. In the longer term, without a method of stabilizing the patella against the femur throughout a series of tests, and being able to replicate this stabilization with multiple transducers in a given knee as well as from knee to knee, it appears that cadaver specimen testing will not yield repeatable or reproducible measurements. This may require use of some type of knee brace for

cadaver functional testing, or alternatively, more in vitro testing with an Instron-type device to generate acceptable reproducibility data. Some of this has been performed and is demonstrated in Section 6.2.

# Chapter 6

# FOLLOW-UP STUDIES

The human knee specimen testing described in the previous chapter was intended to provide final proof of principle for the transducer design, and pave the way for further development of an on-board telemetry system and eventually a self-generating power system. In reality, the human specimen testing revealed fundamental design flaws in the prototype transducer in terms of temperature sensitivity, and systemic problems with the way the transducers were being incorporated into test systems. This testing created multiple hypothesis regarding the device and its use: First, that transducer temperature must be stable throughout the course of a given experiment; second, that ambient temperature changes must be minimal; and finally, that patellar orientation (and thus incident force angle) is important to control. Literally dozens of experiments were conducted as follow-up to the human segment testing in an effort to test the above hypotheses, and discover additional information about the behavior of the transducers. It would be exhaustive, and often unproductive, to detail each experiment that was conduct toward these means. Instead, this chapter focuses on the experiments that effectively address the experiences from the human specimen studies and that provide insight into the nuances of this device.

## 6.1 Testing With The Instron Loading System

Device repeatability was tested using the Instron loading system at the UCHSC Biomechanics Laboratory, allowing for greater control over applied load, direction of load application and device temperature. Both transducers tested in human leg segments were evaluated in this experiment. Transducers were equilibrated to room temperature

for 1.5 hours prior to any testing. Each transducer was set in the test fixture for normal loading and aligned with the Instron device without power applied to the transducer. Once the test setup was ready, the transducer was connected to power, data was captured with the transducer unloaded for five seconds at 10 Hz, and the first loading cycle was immediately initiated. Each transducer was loaded to 200 N using a triangular wave form at 0.1 Hz—six load cycles were performed for each test run. Following completion of a test run, the transducer was disconnected from power and unloaded. The transducer was allowed to set at room temperature without power for five minutes, and then the loading process was repeated. Each transducer was loaded in this fashion five times.

Transducer output data was converted to force using the calibration matrices for each transducer, as described in Chapter 2. Data was analyzed qualitatively by visually assessing the measured load over time as compared to the reported Instron load, and quantitatively by calculating the slope of the measured transducer force versus the reported Instron Load. A graph of the measured load over time from Transducer 1 is shown in Figure 6.1; the slope values and subsequent analysis is shown in Table 6.1. The most noticeable aspect of this data is that the transducers report a maximum measured force that is approximately 35% greater than the maximum applied force reported by the Instron—indicating that the transducers are no longer properly calibrated against the Instron device. Interestingly, the two transducers are in agreement with one another, with Transducer 2 reading about 5% higher than Transducer 1. One would not expect the transducers to drift out of calibration identically, as they seem to have done. The repeatability of each transducer over the five loading runs was calculated using the slope of the measured force versus the reported Instron Force, and by determining the coefficient of variation (%CV) of that value over the five runs. For Transducer 1, the %CV was 2.4%, and for Transducer 2 it was 0.9%—indicating good precision and repeatability for each transducer.

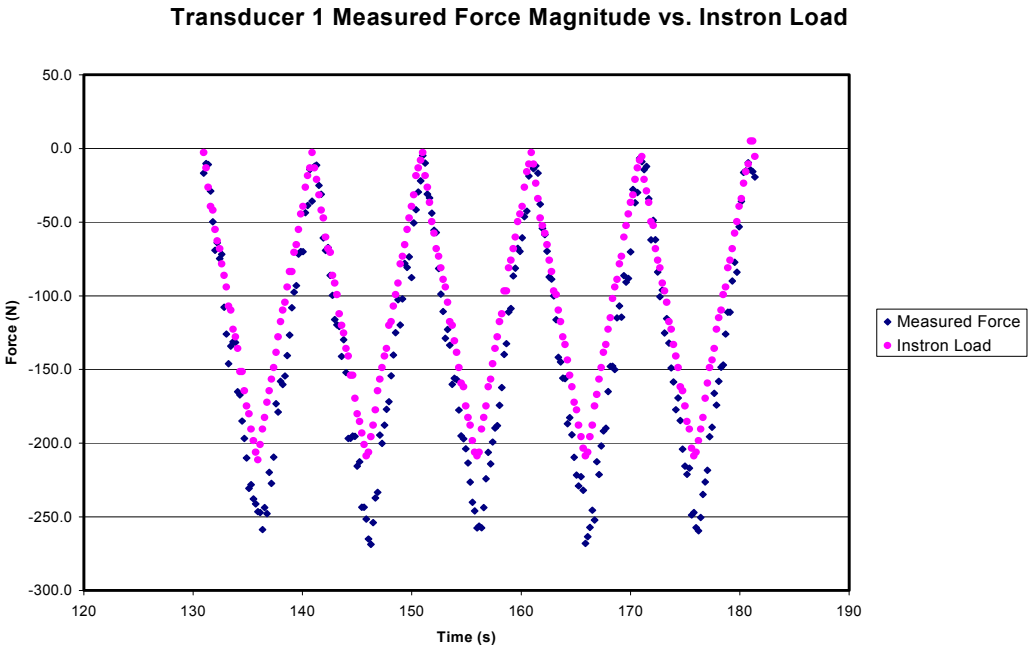


Figure 6.1: Transducer 1 measured force and reported Instron load; run 1 of 5.

| | Transducer 1 | Transducer 2 |
|---|---|---|
| Run 1 | 1.3373 | 1.433 |
| Run 2 | 1.3311 | 1.4072 |
| Run 3 | 1.3333 | 1.4214 |
| Run 4 | 1.3729 | 1.4056 |
| Run 5 | 1.4074 | 1.4278 |
| Mean | 1.3564 | 1.419 |
| St. Dev. | 0.0332 | 0.0122 |
| %CV | 2.4% | 0.9% |

Table 6.1: Slope of the measured force versus reported Instron force. A slope of 1.00 would indicate perfect calibration of the transducers to the Instron device.

The poor correlation of the measured force to the Instron load is troublesome as this is the same device used to calibrate the transducers, and which previously showed good correlation with an applied normal load (Figure 4.8). No relevant changes have been made in the signal processing circuit or in the data acquisition software since calibration was performed. Temperature effects are accounted for in the calibration procedure by normalizing to gage output at a zero load condition; they are then accounted for in individual loading tests by taking an unloaded transducer output measurement and subtracting it from the loaded output. While this relationship will not hold over large temperature ranges due to non-linearities in the strain gages, the gages do respond linearly to changes in temperature over the generally accepted range of "room temperature" (15-24C), as demonstrated in Section 6.3. Therefore, differences in temperature at the time of calibration as compared to the time of this testing should have no impact on measured force. It is possible that the mounts between the gages and the metal plate have degraded over time, but the likelihood of both transducers degrading identically is minimal. A possible cause of the calibration discrepancy is improper calibration of the Instron instrument, either at the time of calibration or at the time of this testing. Calibration records for the instrument were current at the time of both sets of testing, so this is likely not the source of error. Assuming the calibration of the transducers truly does drift over time, this is not a viable transducer for clinical use and appropriate work must be undertaken to correct the problem.

### 6.2 Testing Using A Mechanical Knee

During the first phase of this project a mechanical knee simulation fixture was built for use in testing the eventual transducer design. Due to concerns regarding deviations from normal knee kinematics and the delayed development of the transducer prototype, the fixture was never used for this intended testing. The mechanical knee is being used

now for transducer loading because its geometry is closer to an actual knee than the Instron system, and because testing can be performed in a temperature-controlled environment—unlike a human knee specimen. The mechanical knee consists of a plastic femur mounted to a stationary steel frame, and a tibial component that slides on a curved rail. The knee consists of a TKA prosthesis, and is held together by rubber bands. The original design had a reinforced rubber belt acting as both the patellar and quadriceps tendon, and a free-weight stack was loaded off the distal end of the belt. Belt attachment points to the tibia, patella and femur were taken from nominal kinematic data. The original mechanical knee assembly is shown in Figure 6.2. Initial tests with the assembly indicated that the rubber belt was not sufficient to support weight greater than 30 lb, so it was replaced with steel cable.

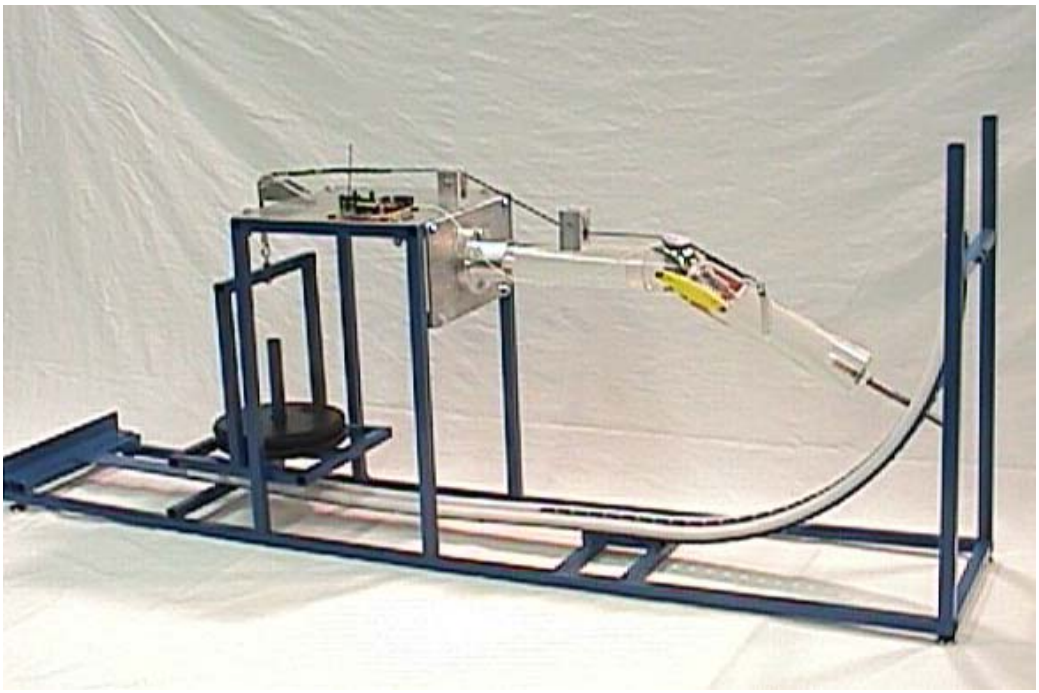

Figure 6.2: Mechanical knee assembly.

The two transducers, the StrainLink board, and the mechanical knee were allowed to equilibrate to room temperature for 1 hour. Room temperature was monitored with a temperature data logger (Dickson Corporation, Addison, IL) at 0.1 Hz, the highest data rate the logger is capable of. The first transducer was fitted into the nylon patella of the mechanical knee using minimal contact with the transducer—this was done to minimize heat transfer to the device. Power was supplied to the transducer and StrainLink and the system was allowed to warm-up for 30 minutes. Output data was checked after the warm-up period to verify that the output was stable. Baseline transducer output was collected at 0.1 Hz for 1.5 minutes. The "quadriceps tendon" was then loaded with 20 kilograms, and the flexion angle was adjusted to 30 degrees (from fully extended). Data was collected at 0.1 Hz for approximately 1.5 minutes. The flexion angle was then adjusted to 60 degrees, and then 90 degrees, with data collection occurring at each angle. Following the 90 degree angle, the load was removed, the fixture was returned to the 30 degree orientation, and the patella was deflected so the transducer was facing away from the femoral surface and unloaded. The transducer was left in this position for 15 minutes, while data was collected at 0.1 Hz. The transducer was then turned back into position and the apparatus was reloaded, and the loading cycle at various angles was repeated. This entire process was repeated for three full loading/unloading cycles for each transducer.

Force magnitude and direction were calculated using the average value for a given run at a given flexion angle, and the pre-run transducer baseline output. The measured force values are shown in Table 6.2. Temperature on the deck of the mechanical knee was $22.5 \pm 0.1\ ^{o}C$ throughout the experiment. The unloaded transducer output drifted an average of 120 counts over the 15 minute rest period—corresponding with a net measured force of 16N. As a comparison, the noise level of the transducer output corresponds with a net measured force of 11N. Analysis of the individual transducers reveals that the repeatability of a measurement within a given transducer is quite good,

with coefficients of variation ranging from 1.8% to 11.8%. Comparison of transducer 1 to transducer 2 reveals significant differences in measured contact force. In addition, the correlation between force and flexion angle is linear for transducer 1, and quadratic for transducer 2—the exact opposite from what was observed in the human leg segment testing. Measured force as a function of flexion angle is represented graphically in Figure 6.3.

**Transducer 1**

| Angle | Run 1 | Run 2 | Run 3 |
|---|---|---|---|
| 30$^o$ | 43 | 48 | 54 |
| 60$^o$ | 97 | 83 | 106 |
| 90$^o$ | 138 | 139 | 143 |

**Transducer 2**

| Angle | Run 1 | Run 2 | Run 3 |
|---|---|---|---|
| 30$^o$ | 84 | 98 | 94 |
| 60$^o$ | 176 | 167 | 172 |
| 90$^o$ | 170 | 168 | 151 |

Table 6.2: Measured force from mechanical knee testing with 196 N quadriceps load.

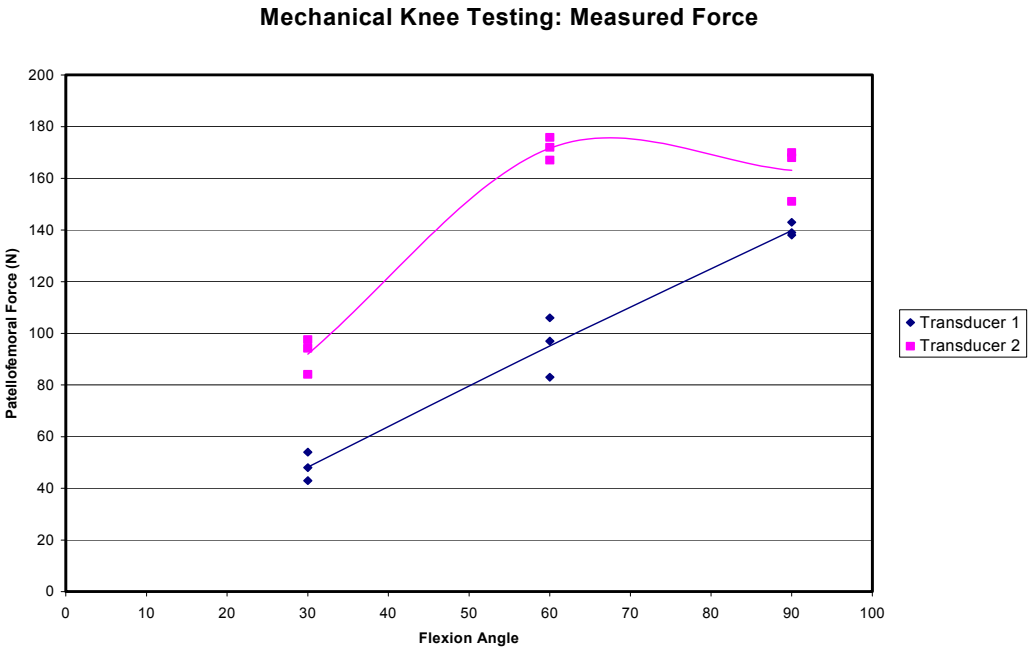


Figure 6.3: Measured patellofemoral contact force in mechanical knee fixture.

The testing in the Instron loading device described previously indicates that the transducers are reading identically to each other, but that they are out of calibration by approximately 30%. In contrast, this data (and the human knee data) suggest that the two transducers are functioning differently relative to each other. One explanation for this inconsistency is the difference of incidence angles of the load in the two systems. The Instron applies load directly through the center of the transducer—in this case it is a fully normal load. This is the optimal measurement situation for the transducer, as the load is applied directly in the center of the three-gage rosette, and is equidistant from the three calibration vectors. The human knee and mechanical knee cases involve incident angles that are often outside of the three calibration vectors and loads that do not necessarily project through the center of the device. These differences in the way the devices are loaded may account for the differences in behavior between the two transducers. While

this reasoning does provide a logical (though theoretical) explanation for the inconsistent relationship between the reported forces for the two transducers, the expectation from two calibrated measurement devices is that they measure the same force equivalently. It is unclear whether this discrepancy represents a flaw in the calibration procedure or with the transducer design.

### 6.3 Transducer Thermal Stability

Transducer output drift has been observed from the onset of this phase of the Telemetric Knee project. Significant effort was expended early in this project to characterize and eliminate drift, temperature effects, self-heating, and other sources of noise. However, it seems that the problem is persistent, and may have been reintroduced when the StrainLink system was incorporated into the program. Several studies have been conducted to determine the cause of the fluctuating background signal, including temperature stability, temperature dependence, and load repetition studies.

Prior to testing, the human leg specimens were stored in refrigeration at $4^{o}$C, while the transducer was stored at room temperature (approximately $22^{o}$C). The transducers were placed in the leg specimens and allowed to set for 30 – 60 minutes, allowing some temperature equilibration. Still, the leg had not yet warmed to room temperature, so the system was constantly warming throughout testing. This is believed to be the primary source of variation in the human knee studies described previously. To determine the sensitivity to temperature, a small amount of water at $4^{o}$C was placed at room temperature with a patellar transducer submerged in it. Data was taken from the transducer, along with temperature, as the water warmed to $15^{o}$C. This data shows a large change in gage output from $4^{o}$C – $15^{o}$C (Figure 6.4), indicating that large temperature swings during testing would be problematic. It is noted that the

transducer/leg system may well have been at 15°C when testing was started, and warming during the testing would then be between 15°C and 22°C—outside the range investigated here. Also, warming in that range would occur more slowly than in the lower range, suggesting less of an impact on transducer output. This temperature effects test is likely a poor model for the temperature variation that occurred during cadaver feasibility testing, nonetheless, it provides indications of the effects that temperature can have on transducer output.

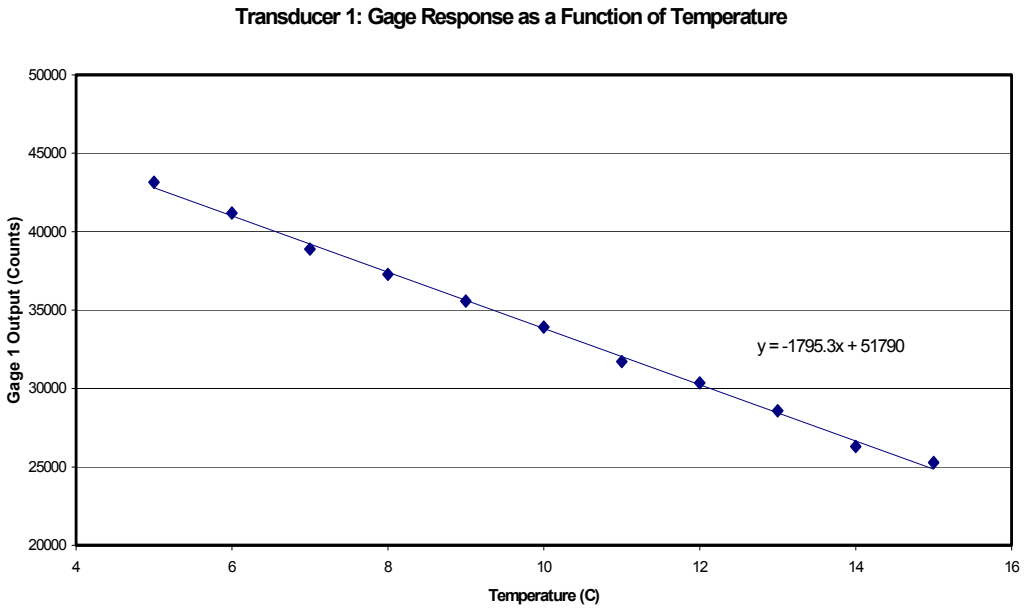


Figure 6.4: Gage 1 output from transducer 1 while submerged in water warming from 4°C to 15°C.

As a follow-up, the system was tested in an incubation cabinet (Helmer Labs, Noblesville, IN) between the temperatures of 13°C and 24°C, a range that represents the typical interpretation of "room temperature". The temperature set-point of the chamber

was changed from the low point to high point and was oscillated between these set-points 3-5 times per experiment. It would take the chamber anywhere from 30-60 minutes to adjust to the new set-point, depending on ambient room temperature and whether the incubator is heating (longer equilibration time) or cooling (shorter time). This study was conducted with both the transducer and the StrainLink board in the incubator, with the transducer completely unstrained. The data for both transducer 1 (Figure 6.5) and transducer 2 (Figure 6.6) indicate that small changes in temperature have a large effect on transducer output—for transducer 2, a $1^{o}$C temperature change corresponds with a 300N change in measured force. One point of note is the hysteresis seen in transducer 1 that is not evident in the data set for transducer 2. Because there is only one data acquisition system, the two transducers must be tested separately, and in fact they were tested on different days. The ambient temperature for the runs was not recorded, but the equilibration time for the run with transducer 2 was (on average) 17% slower than for transducer 1, indicating a possible capacitive affect on the strain gage response. In fact, the reason for this phenomenon is not known, and in repeat studies, the hysteresis effect was present for both transducers. In these studies temperature equilibration time was similar to the temperature effects in the first run with transducer 1.

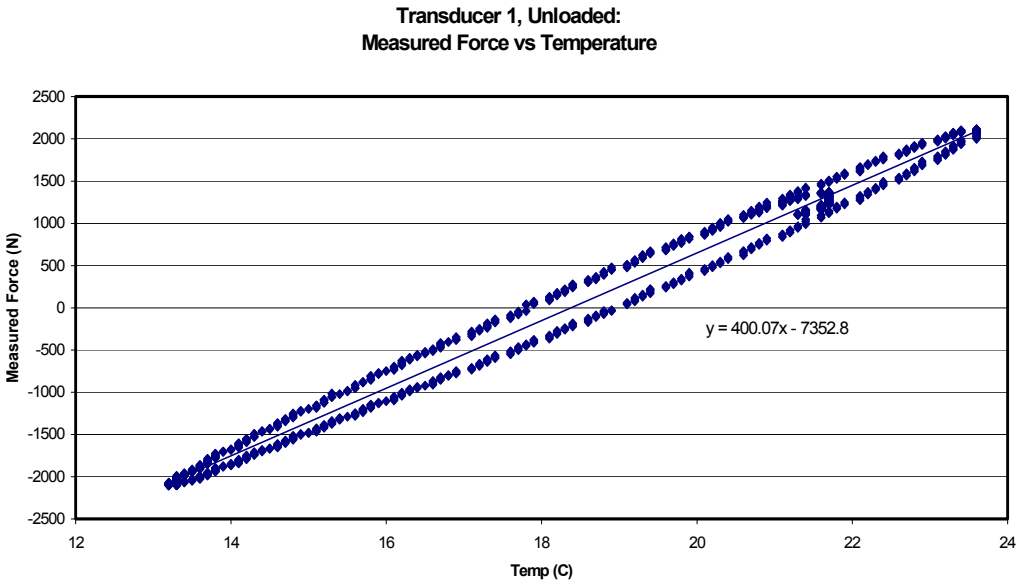


Figure 6.5: Force measured by transducer 1 while unloaded from 13°C to 24°C.

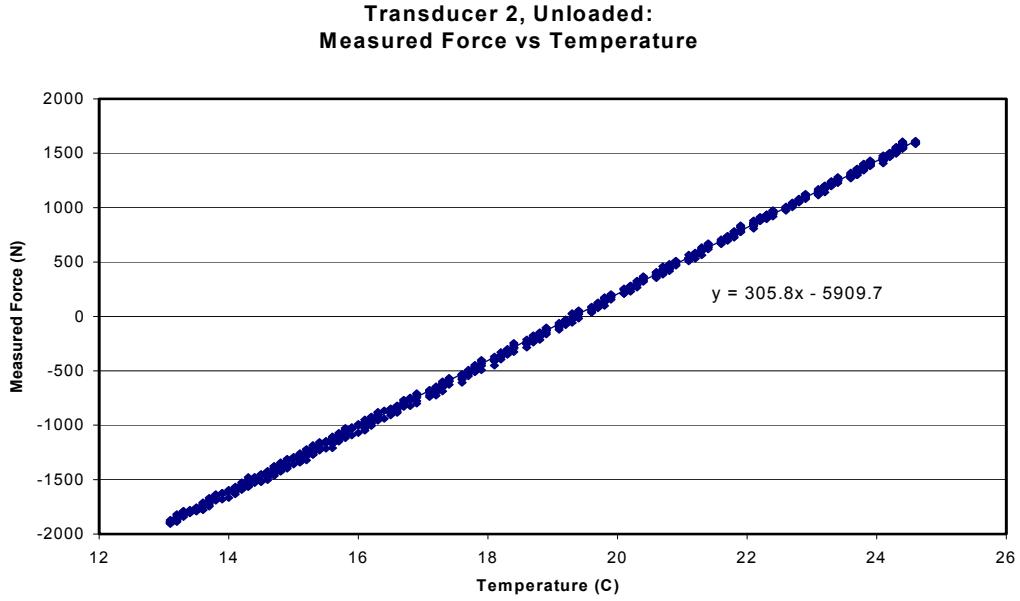


Figure 6.6: Force measured by transducer 2 while unloaded from 13°C to 24°C.

The above studies regarding temperature effects upon transducer output indicate that small changes in device temperature are associated with large changes in transducer output, leading to a performance specification that is entirely unacceptable for the intended application. While great measures could be taken to conduct *in vitro* and *in situ* tests at near-isothermal conditions (± 0.2$^{o}$C), the *in vivo* application will likely experience temperature changes on the order of ± 2$^{o}$C, if not larger—which, according to the data presented in Figures 6.5 and 6.6, corresponds with forces in excess of ± 600N. This clearly suggests that the device cannot be used for its intended application without some type of hardware mediated temperature-compensation circuitry. This will be discussed in more detail in Chapter 7.

Previous testing with the transducers had indicated that there was a self-heating phenomenon when the transducer was first connected to power. To test and quantify this effect, transducer 1 and the StrainLink system were equilibrated in the incubator at 22$^{o}$C overnight, without power. The system was then connected to power and gage output data was immediately acquired. Once again, all three gage channels responded equivalently—only the data plot from channel 1 is presented here in Figure 6.7. As was done with the temperature-variation experiment, gage output was converted to a theoretical force measurement, as illustrated in Figure 6.8. This data suggests the same 20-30 minute stabilization time that was observed previously in both *in vitro* testing and human leg specimen testing. The measured force value of 500 N indicates that this self-heating phenomenon is significant and can cause errors in the measured force if not accounted for.

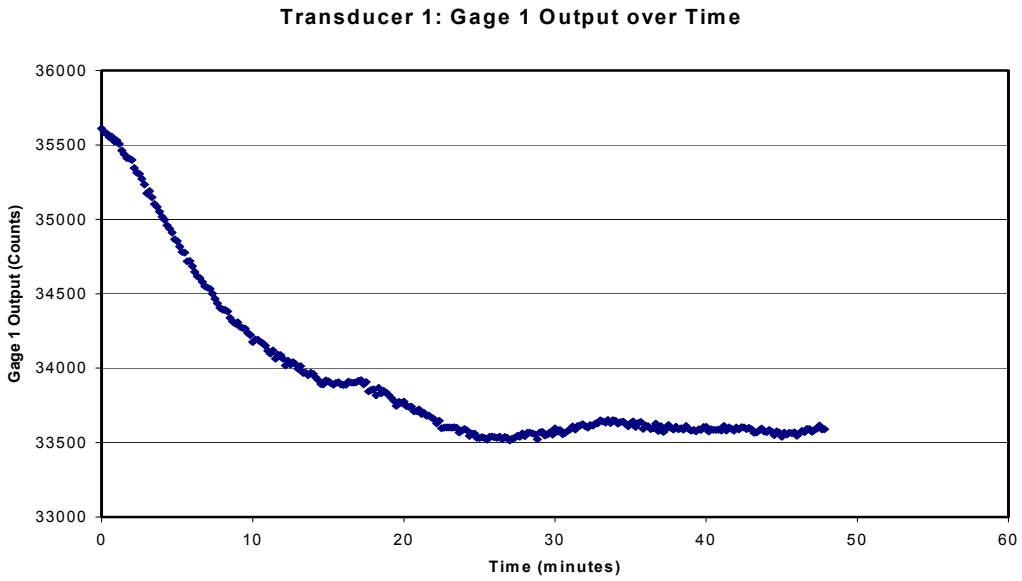


Figure 6.7: Gage output of transducer 1—self-heating effects.

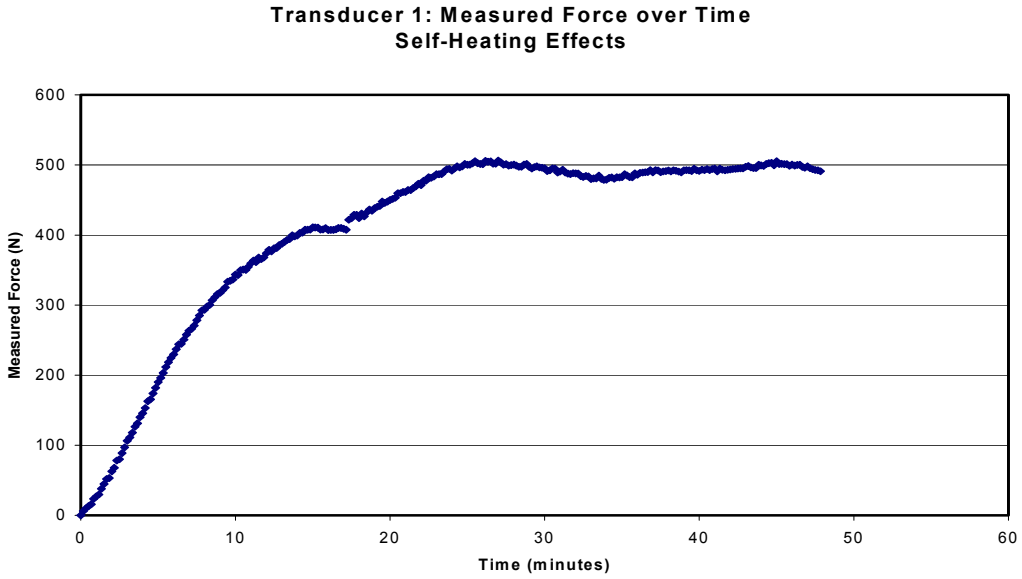


Figure 6.8: Force measured by transducer 1 due to self-heating effects.

### 6.4 Temperature Compensation

The data presented thus far in this chapter indicate that the lack of temperature compensation within the transducer is a primary source of measurement error. While it is not possible to add temperature compensation to these transducers without redesigning and rebuilding, it is possible to simulate it on the StrainLink signal processing circuit. The balance resistor for each Wheatstone bridge was removed and replaced with a transducer gage channel with a resistance that matches the baseline resistance of transducer 2. Channel 2 of transducer 1 and channels 2 and 3 of transducer 4 were used as the balance resistors. All three resistors were placed in the incubator (Helmer Labs) at 22$^{o}$C and allowed to equilibrate without power for one hour. Power was then supplied to the system and data was immediately acquired—not allowing a warm-up period to account for the initial self-heating. The set-point of the incubator was then dropped to 13$^{o}$C. Once at 13$^{o}$C, the set-point was reset to 22$^{o}$C. This was repeated for one additional cycle. The resulting net measured force versus temperature profile is shown in Figure 6.9.

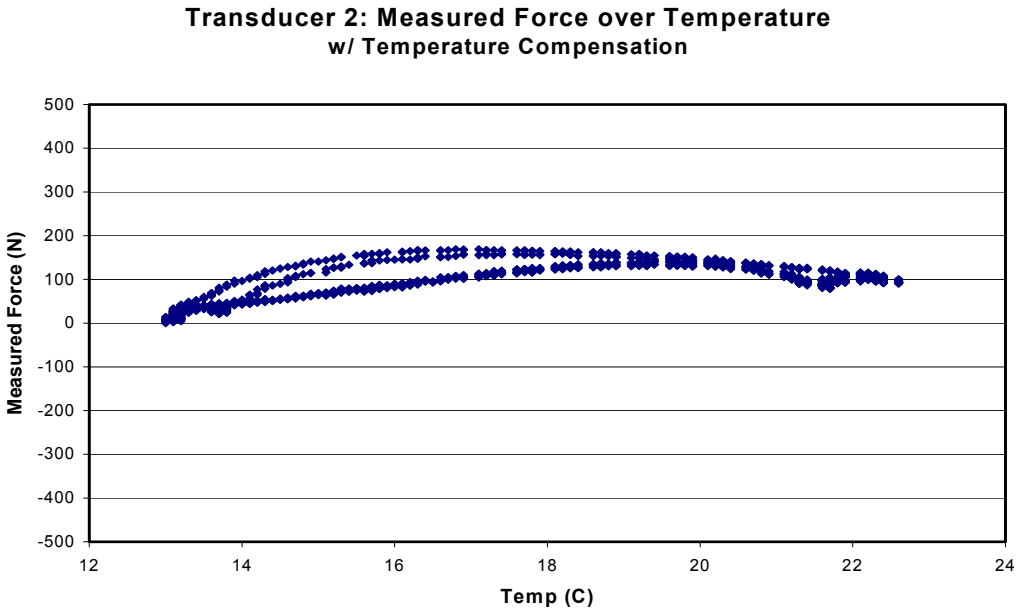


Figure 6.9: Force measured by transducer 2 over variable temperature with temperature compensation gages.

Once again, the device demonstrates significant hysteresis—but unlike previous experiments, the net measured force is rather constant over the tested temperature range. This result is not unexpected, as the resistance of the balance gages will change with temperature at the same rate as the test transducer gages. The indication is that proper temperature compensation techniques, either for each individual channel or for the transducer as a whole, will mitigate much of the measurement error that has been seen throughout this phase of the project. The implementation of this circuitry is not trivial however, and is reserved for future phases of this project. Several possible methods of implementation are presented in Chapter 7.

# Chapter 7

# FUTURE WORK

Work performed to date on this Telemetric Knee System has indicated that the concept and current path are both feasible and obtainable. The current transducer and telemetry system design meet the design input requirements for transmission distance, sample frequency and sensitivity, although the temperature instability of the transducer is unacceptable. In addition to correction of temperature sensitivity/stability issues, work must be done to miniaturize the telemetry system to encase it in the patellar transducer, which will also require some redesign of the transducer to expand the cavity. Currently, the entire system is powered by a conventional 9-volt battery, which clearly is not an acceptable final power source. Ultimately, there is a desire to have this device be self-powered, i.e.: incorporate a chemical or kinetic power generator. Finally, there are still concerns regarding the calibration system, both in ease-of-use, as well as reliability. These issues must be addressed before the design can be finalized.

## 7.1 Temperature Stability

Temperature has been shown to be a primary cause of virtually all of the aberrant measurements observed with the patellar transducer design. Currently there is no mechanism for correcting for ambient temperature, causing highly variable output readings when doing tests in non-isothermal environments. Because the device is so sensitive to temperature, even temperature fluctuations of $\pm 1^{o}C$ cause noticeable differences ($\pm$ 300N) in device output. Furthermore, there is a transient self-heating effect over the first 20-30 minutes that the system is connected to power. If the device is to be constantly powered this is not of concern, but both primary options for power

source are discontinuous, making this self-heating phenomenon unacceptable in the final design.

Strain-based force measurement systems, such as the one used in this design, typically handle temperature variation by incorporating an extra strain gage, mounted in an unstrained position, that is used as a blank to subtract off changes in temperature. Because the gage is mounted in an unstrained location, any change in output is logically due to changes in temperature. This output fluctuation can then be removed from the active strain gages, thus offsetting the temperature drift. For this specific application, there is little opportunity for mounting a gage in an unstrained location. The inner surface of the backing plate may be a good candidate location, but the exact loading profile of this surface has not yet been analyzed. In addition, the strain seen at this point will be highly dependent on the bone-metal contact area, and therefore may be widely variable. Furthermore, because the intent is to implant electronics into the transducer cavity, the temperature on the transducer-plate surface may not be the same as the temperature on the backing-plate surface, thus negating any benefit of this temperature offset configuration. If this method is indeed incorporated, it would be best to perform FEA on the laser-welded transducer to determine the strain profile on the inner surface of the backing plate. In addition, it would be necessary to evaluate the temperature profile of the telemetry electronics to determine if the temperature at the two surfaces would vary comparably. Both of these evaluation steps would require a completed design of the embedded telemetry system, and would therefore need to be performed later in the project.

A second option is to incorporate a traditional temperature measurement system, such as a bimetal thermocouple, and calibrate it against the gage rosette output. Any thermocouple used would have a different response profile than the strain gages, which would require a relationship to be determined between the two measurement systems. This obviously creates the disadvantage of requiring a second calibration step for each

transducer, increasing the cost and decreasing the ease of device manufacture, and adding an additional mode of error. While the strain gage system mentioned previously would account for self-heating effects, this method would not. The advantage of this method is the lack of need for an unstrained surface for mounting. In fact, the thermocouple could potentially be mounted anywhere in the device and function appropriately.

A third method for temperature control in a final device configuration is to incorporate a matched strain gage into the Wheatstone bridge circuit for each channel, which would be located on the telemetry circuitry embedded within the transducer. Assuming the geometry is assessed correctly, the balance gages could be placed in close relation to the sensor gages, allowing for accurate temperature sensing at each gage location. By placing the balance gages on the telemetry circuit, the unstrained requirement is assured, and incorporation into the bridge circuit insures proper self-heating offset. One drawback to this is that it will only work for a fully embedded signal processing circuit, and therefore will be very difficult to test without actually building. Another issue is that the gages mounted to the patella will potentially change temperature at a higher rate than the gages mounted to the telemetry board. It would be possible to test the principle by designing a 3-bridge processing circuit to be embedded in the transducer, while maintaining all of the telemetry outside of the transducer. This would require an additional design step upfront, and the added expense of additional prototypes, but would avoid the steeper expense and design time surrounding telemetry miniaturization for a system that may not work.

### 7.2 Telemetry System

The current StrainLink telemetry system was used to test the principle of the telemetric knee concept, and to establish a comfort level with the technology provided by MicroStrain Inc. This system will not work in a final design as it is simply too large to fit

within the constraints of the patella. When the decision was made to use MicroStrain as the telemetry provider, it was understood that a custom system would need to be designed to fit within the patellar transducer once a final design was reached. The platform for the MicroStrain telemetry system for the patellar transducer is their EmbedSense transceiver. The dimensions of the production version of EmbedSense are not compatible with that of the patellar transducer, but the design team at MicroStrain believes they can take the inductive coil off-board and reduce the circuit size to approximately 0.75 in. diameter and 0.125 in. thickness. The current cavity in the transducer is 1.25 in. diameter and 0.035 in. deep. Recovering a minimum of 0.09 in. depth within the cavity will likely be difficult, but a preliminary evaluation of the transducer design indicates that it is possible. As much as 0.025 inches can be recovered from the backing-plate, leaving 0.065 to be recovered from the transducer plate. The current transducer plate design was obtained from FEA analysis in an effort to maximize polyethylene volume and contact area, as well as maximize strain and minimize stress. By compromising some on polyethylene volume and reducing the contact area on the inner surface of the transducer outer ring, the cavity should be able to be expanded without decreasing sensitivity or fatigue resistance.

The dimensions provided by MicroStrain for a final device were done with minimal design time and no regard for changes in functionality from the EmbedSense platform. In reality, the patellar transducer will require 3-channel telemetry, while the EmbedSense is designed to provide up to twelve channels—this reduction in functional requirements could potentially reduce the size of the transmitter. In addition, circuit design advances in the 18-24 month period between the initial dimension quote and likely circuit design timeframe could reduce the space demand by as much as 30%--this is based upon a reported 50% size reduction in the 24 month period leading to the release of EmbedSense. Finally, Microstrain was asked to reduce the device size as much as possible; they did so by reducing both the diameter and thickness proportionally. The current transducer design has more than enough diameter space to accommodate a

telemetry system, so there is some chance that the thickness can be reduced by expanding the diameter. In summary, the cited dimensions quoted by MicroStrain should not be used as a definitive mark for transducer redesign, but rather should be noted when the dimensions of both the backing plate and the transducer plate are reevaluated. Once a reasonable design is established that provides a larger cavity without compromising sensitivity or strength, and with minimal compromise of polyethylene volume, this dimension should be forwarded to MicroStrain for formal design consideration. Additional transducer plate redesign may be necessary, but ideally it would be minimal.

A final consideration regarding the telemetry circuitry is the method of mounting it in the transducer cavity. Assuming the final design will incorporate matched strain gages on the telemetry board as described in the latter part of Section 7.1, it is ideal to mount the board in close proximity to the transducer plate inner surface, allowing for a small degree of flexion—on the order of 0.01 in. from the plate surface. The board should be physically mounted to the backing plate using cast mounting rivets and standoffs, or the equivalent. Clearance from the backing plate is less critical, but must be large enough to prevent electrical contact or arcing; 0.005 in. should be sufficient. Obviously these spacing requirements necessitate an even larger cavity within the transducer, furthering the need for an optimized telemetry circuit design

### 7.3 Power System

A primary area for future research is with a power system for the device. As described in Section 7.2 above, there is little available space in the transducer cavity for incorporation of a telemetry system, and no space for a kinetic power system. Use of a kinetic generator would require a moving weight, an inductive coil, and a capacitance system, all of which is space consuming. A further complication is that the weight seemingly must move in the ventral-dorsal plane, a space that is currently 0.035 in. deep,

and will eventually have a circuit card embedded in it, not leaving much room for motion of a weight. There are other possible alternatives including an orbiting weight mounted laterally on a semi-stiff spring or a bi-density fluid system—both of which introduce many potential complications and sources of failure. Other less complicated options may either be available, or become available, over the course of continued investigation.

The current design suggestion involves the inductive power system provided by MicroStrain as part of the EmbedSense platform. Due to space restrictions and transmission concerns, it is suggested that the coil be moved off of the telemetry circuit and be mounted subcutaneously on the outside of the knee capsule. The coil would be flexible, approximately 1.5 in. diameter and 0.03 in. thick, and could be encased in a protective plastic coating. The wire lead would access the telemetry electronics in the same fashion as the gage lead currently exits the transducer, from an access hole in the backing plate that is hermetically sealed. While this is clearly not an optimal design, it is functional, has minimal implementation hurdles, and is consistent with other induction-powered implanted devices [24, 36]. Theoretically, telemetry could be conducted through this induction coil as well, but it is recommended to retain the radio telemetry (if space permits) so that when a self-powered system is ready the telemetry system does not require redesign.

### 7.4 Further Calibration Work

The calibration data presented in Chapter 4 for the angled calibration fixture indicated that calibration was repeatable for a given transducer, and that it held for incident forces not related to the calibration routine. However, subsequent testing using the Instron instrumentation illustrated that the calibration had not held over time (Section 6.1). Furthermore, in both human specimen testing and mechanical knee testing, transducers 1 and 2 reacted differently to what should have been equivalent net contact

forces. This is in contrast to the data collected on the Instron which suggested that both transducers measured the same applied force, although it was measured incorrectly. These findings may simply be a byproduct of other issues with the transducer design that have previously been cited, but may also indicate a potential problem with the calibration procedure. There is little use in revisiting calibration with the current transducer design as gage mounting concerns and temperature instability are not accounted for. However, it would be prudent to spend significant time with the next-generation transducer prototype verifying that calibration is repeatable, and that known applied loads of various magnitudes and incident direction are recoverable.

Additional concerns with the current calibration procedure involve the physical set-up and the ease of use of the procedure. The current instrumentation setup requires a considerable amount of "eyeballing", which is potentially a source of significant error. There is currently no alignment fixturing to insure that the Instron applies load along the same vector each time, and that every transducer is fixed in the instrument identically. Once calibration data is obtained, significant time and three software applications are necessary to analyze the data and produce a calibration matrix. Furthermore, as discussed previously, the MatLab routine for forming the matrix normalizes the data so the y-intercept is zero. This was done to compensate for temperature effects between runs, but was also done to simplify the matrix mathematics. From a practical standpoint, this system yields an almost useless calibration routine, as an unloaded transducer output value is unobtainable in an implanted device. Both the painstaking data manipulation and the normalization of calibration curves must be removed from the calibration procedure before the Telemetric Knee System design can be considered complete.

## REFERENCES CITED


1. VA Brander, SD Stulberg, AD Adams, RN Harden, S Bruehl, SP Stanos, T Houle. *Predicting total knee replacement pain: a prospective, observational study*. Clinical Orthopedics, 416:27-36, 2003.

2. MJ Hall, CJ DeFrances. *2001 National Hospital Discharge Survey.* Department of Health and Human Services Advance Data from Vital and Health Statistics, 332, 2003.

3. N Bradbury, D Borton, G Spoo, MJ Cross. *Participation in sports after total knee replacement*. American Journal of Sports Medicine, 26:530-535, 1998.

4. S Najibi, R Iorio, JW Surdam, W Whang, D Appleby, WL Healy. *All-polyethylene and metal-backed tibial components in total knee arthroplasty: a matched pair analysis of functional outcome*. Journal of Arthroplasty, (18-1):9-15, 2003.

5. A Godest, S de Cloke, M Taylor, P Gregson, A Keane, S Sathasivan, P Walker. *A computational model for the prediction of total knee replacement kinematics in the sagital plane*. Journal of Biomechanics, 33:435-442, 2000.

6. DD D'Lima, JE Slamin, CW Colwell. *An implantable telemetrysystem to measure intra-articular tibial forces*. Orthopedic Research Society, Anaheim, CA, 1999.

7. KR Kaufman, N Kovacevic, SE Irby, CW Colwell. *Instrumented implant for measuring tibiofemoral forces.* Journal of Biomechanics, 29 (5): 667-671, 1996.

8. CP Townsend, SW Arms, MJ Hamel. *Remotely Powered, multichannel, microprocessor based telemetry systems for a smart implantable total knee implant*. MicroStrain, Inc. White Paper, 1999.

9. GE Holt, DA Dennis. *The role of patellar resurfacing in total knee arthroplasty*. Clinical Orthopedics, 416:76-83, 2003.

10. DR Wilson, MV Apreleva, MJ Eichler. FR Harrold. *Accuracy and repeatability of a pressure measurement system in the patellofemoral joint*. Journal of Biomechanics, 36 (12): 1909-1915, 2003.

11. DD D'Lima, PC Chen, MA Kester, CW Colwell Jr. *Impact of patellofemoral design on patellofemoral forces and polyethylene stresses*. The Journal of Bone and Joint Surgery: American Volume, 85-A Supplement 4:85-93, 2003.

12. MC Dace. *Design, Analysis and Evaluation of a Self-Powered Telemetric Knee*, Colorado School of Mines Graduate Thesis, 2001.

13. BA Morris, DD D'Lima, J Slamin, N Kovacevic, SW Arms, C Townsend, CW Colwell Jr. *e-Knee: Evolution of the electronic knee prosthesis. Telemetry technology development*. The Journal of Bone and Joint Surgery: American Volume, 83-A Supplement 2:62-66, 2001.

14. www.medizin.fu-berlin.de/biomechanik/Prokneee.htm: "Measurements of Knee Joint Forces", 2003.

15. G Bergman, F Graichen, J Siraky, H Jendrzynski, A Rohlmann. *Multichannel strain gauge telemetry for orthopedic implants.* Journal of Biomechanics, 21:169-176, 1988.

16. G. Bergmann, J Siraky, A Rohlman, R Kolbel, *Measuring spatial forces by the "Matrix Method"*. In Proc. V/VI, 9th World Congress, 395-404. IMECO, 1982.

17. F Graichen, A Rohlmann, G Bergmann. *In vivo load measurements with instrumented orthopaedic implants*. 17th International Symposium on Biotelemetry, Brisbane, Australia, 2003.

18. www.bluetooth.com/tech/works.asp: "Introduction to Bluetooth Technology".

19. www.bluetooth.org/foundry/specification/docman/: Bluetooth Specification, V1.1, January 2003.

20. Wu, Q; Esteves, E: The cdma2000 High Rate Packet Data System (2001), www.qualcomm.com/cdma/1xEV/pub_papers/cdma2000_HighRatePacket.pdf.

21. A Abrial, J Bouvier, M Renaudin, P Senn, P Vivet. *A New Contactless Smart Card IC Using an On-Chip Antenna and an Asynchronous Microcontroller*. IEEE Journal of Solid-State Circuits, 36:1101-1106, 2001.

22. NF Guler, ED Ubeyli. *Theory and Applications of Biotelemetry*. Journal of Medical Systems, 26:159-177, 2002.

23. F Burny, M Donkerwolcke, F Moulart, R. Bourgois, R Puers, K Van Schuylenbergh, M Barbosa, O Paiva, F Rodes, JB Begueret, P Lawes. *Concept, design and*

*fabrication of smart orthopedic implants.* Medical Engineering and Physics, 22:469-479, 2000.

24. R Puers, G Vandevoorde. *Recent progress on transcutaneous energy transfer for total artificial heart systems*. Artificial Organs 25:400-405, 2001.

25. J Mullins. *Micro supplies to power MEMS systems*. IEEE Spectrum, Sept:23-24, 2001.

26. SH Reichenbach, GD Egrie, SM Marinache, KJ Gustafson, DJ Farrar, JD Hill. *Sustained skeletal muscle power for cardiac assist devices: Implications of metabolic Constraints*. ASAIO Journal 47:541-547, 2001.

27. T Chen, SC Barton, G Binyamin , Z Gao, Y Zhang, H Kim, A Heller. *A miniature biofuel cell*. Journal of the American Chemical Society, 123:8630-8631, 2001.

28. E Katz, AF Buckmann, I Willner. *Self-powered Enzyme-based Biosensors*. Journal of The American Chemical Society, 123:10752-10753, 2001.

29. S Hirokawa. *Three-dimensional mathematical model analysis of the patellofemoral joint.* Journal of Biomechanics, 24(8):659-671, 1991.

30. GT Yamaguchi, FE Zajac. *A planar model of the knee joint to characterize the knee extensor mechanism*. Journal of Biomechanics, 22(1):1-10, 1989.

31. CS Oishi, KR Kaufman, SE Irby, CW Colwell Jr. *Effects of patellar thickness on compressive and shear forces in total knee arthroplasty.* Clinical Orthopedics, 331:283-290, 1996.

32. R Singerman, J Berilla, DT Davy. *Direct in vitro determination of the patellofemoral contact force for normal knees.* Journal of Biomechanical Engineering, 117(1):8-14, 1995.

33. ML Harris, P Morberg, WJ Bruce, WR Walsh. *An improved method for measuring tibiofemoral contact areas in total knee arthroplasty: a comparison of K-scan sensor and Fuji Film.* Journal of Biomechanics, 32(9):951-958, 1999.

34. JM Bach, ML Hull. *A new load application system for In Vitro study of ligamentous injuries to the human knee joint.* Journal of Biomechanical Engineering, 117:373-382, 1995.

35. DT Reilly, M Martens. *Experimental analysis of the quadriceps muscle force and patello-femoral joint reaction force for various activities.* Acta orthopaedica Scandinavica, 43:126-137, 1972.

36. EL McKee, DP Lindsey, ML Hull, SM Howell. *Telemetry system for monitoring anterior cruciate ligament graft forces in vivo*. Medical and Biological Engineering and Computing, 36:330-336, 1998.

# Appendix A

Calibration Loading Profiles Using the Side-Loading Calibration Procedure

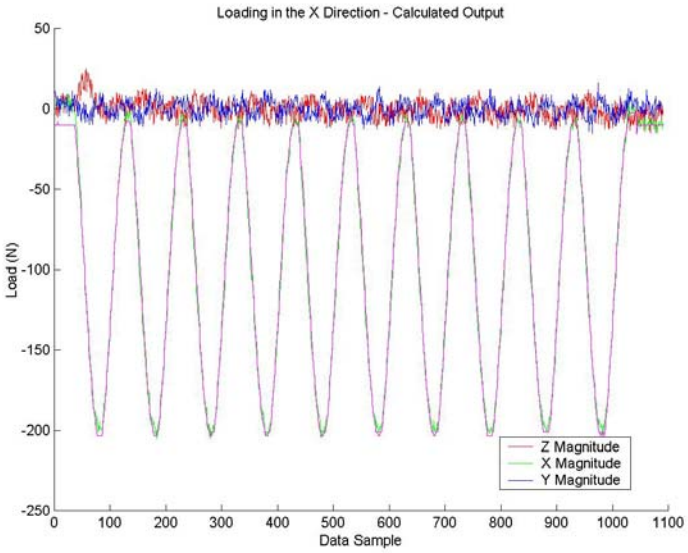


Figure A.1: X-loading profile for calibration run 1

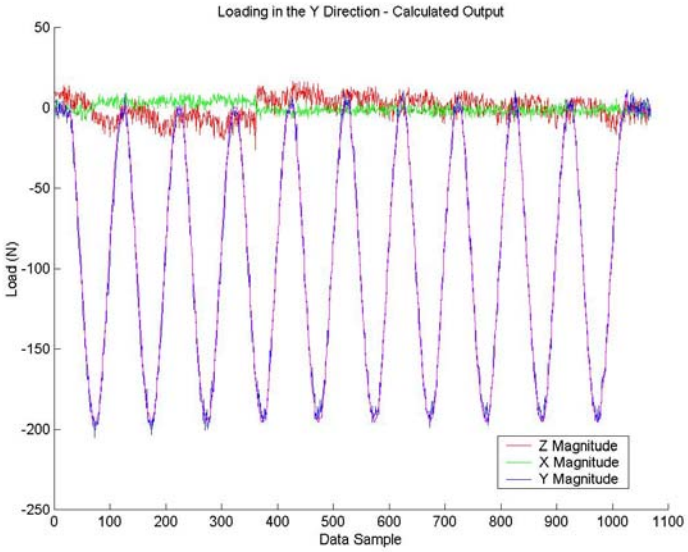


Figure A.2: Y-loading profile for calibration run 1

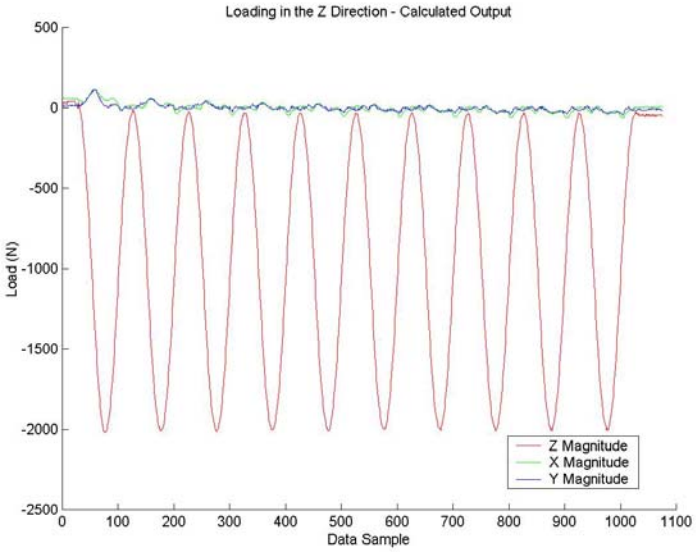


Figure A.3: Z-loading profile for calibration run 1

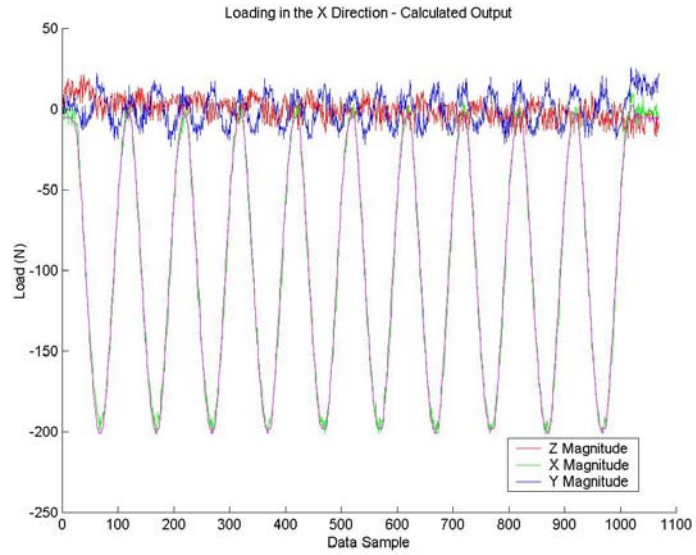


Figure A.4: X-loading profile for calibration run 2

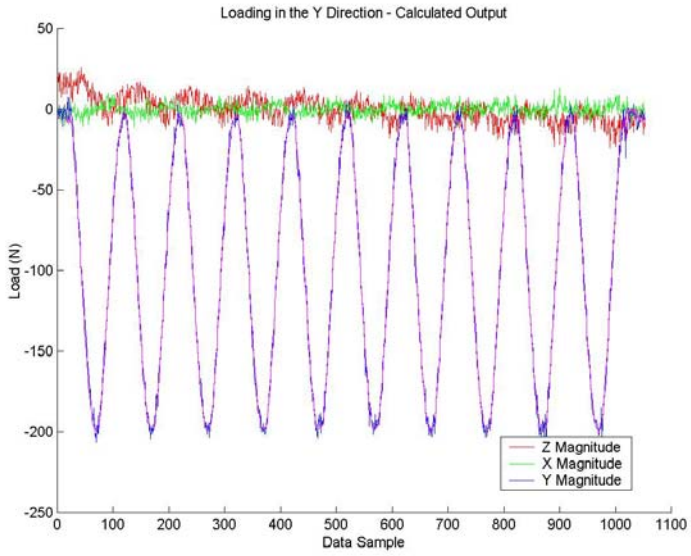


Figure A.5: Y-loading profile for calibration run 2

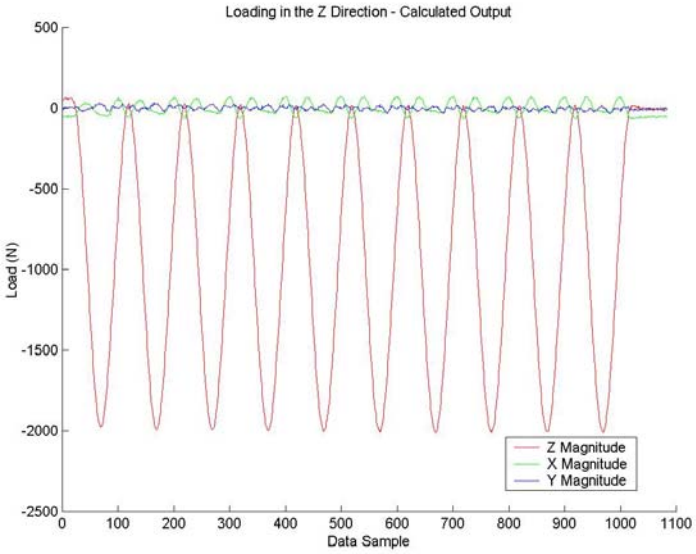


Figure A.6: Z-loading profile for calibration run 2

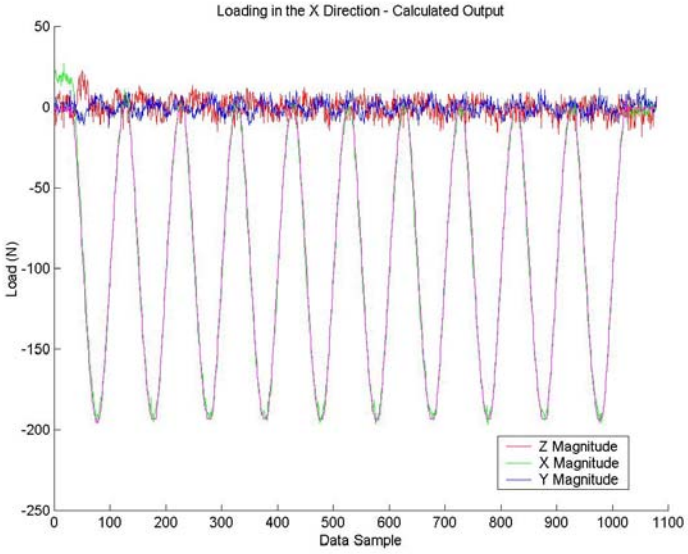


Figure A.7: X-loading profile for calibration run 3

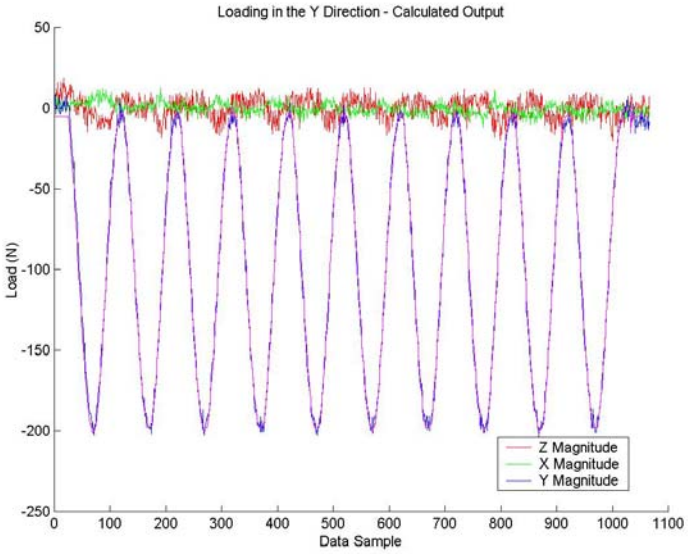


Figure A.8: Y-loading profile for calibration run 3

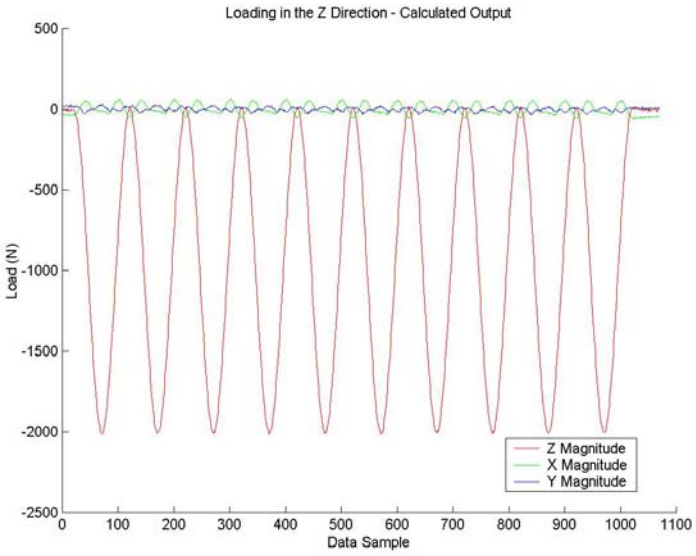


Figure A.9: Z-loading profile for calibration run 3

# Appendix B

Calibration Loading Profiles Using the Offset Calibration Procedure

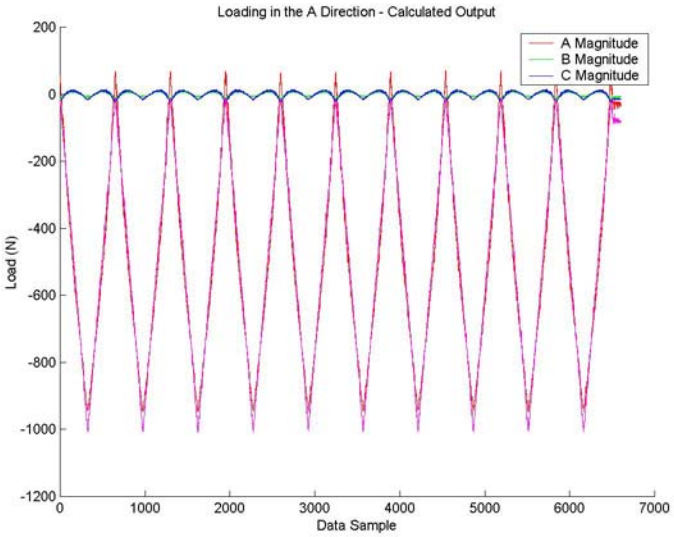


Figure B.1: A-loading profile for calibration run 1

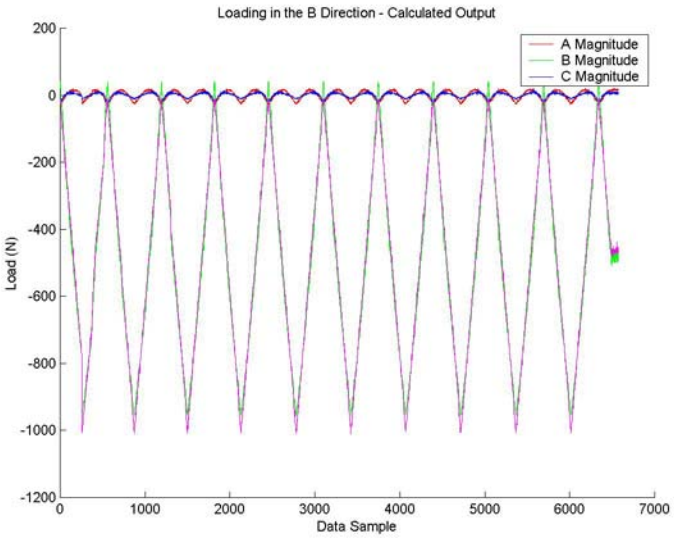


Figure B.2: B-loading profile for calibration run 1

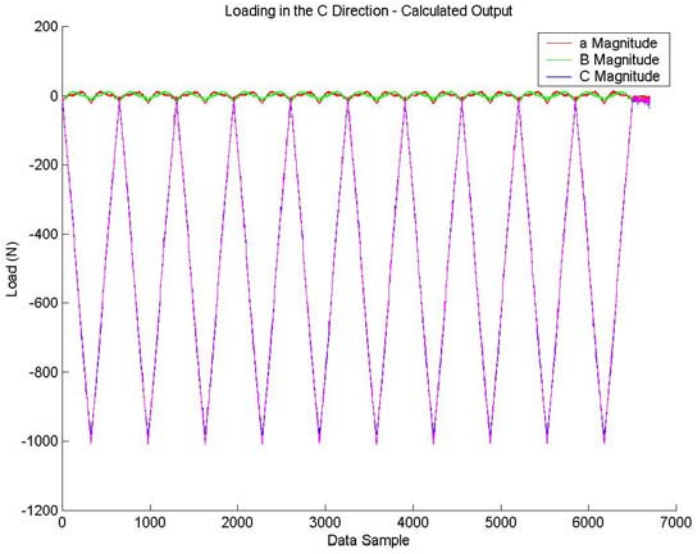


Figure B.3: C-loading profile for calibration run 1

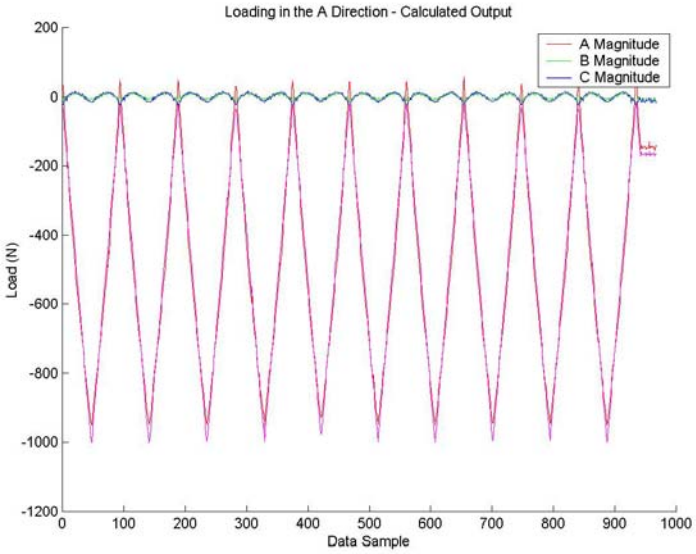


Figure B.4: A-loading profile for calibration run 2

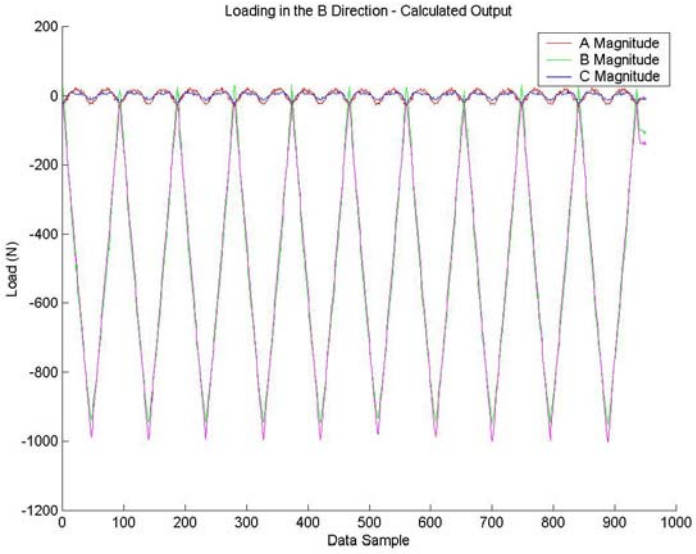


Figure B.5: B-loading profile for calibration run 2

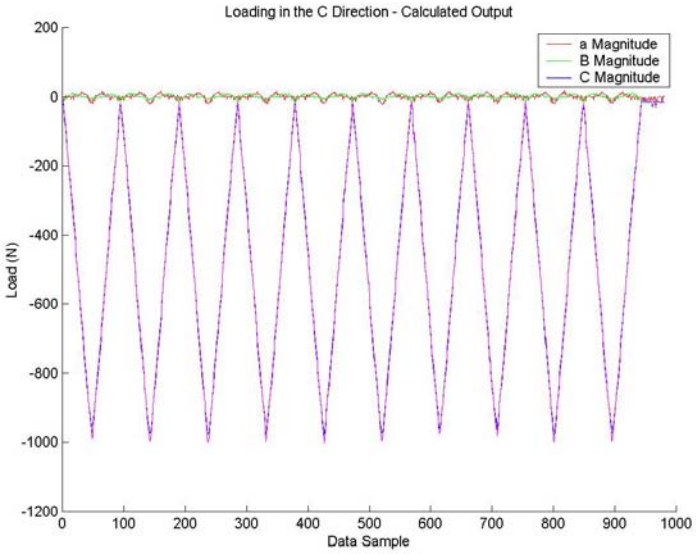


Figure B.6: C-loading profile for calibration run 2